Physical Oceanographic Processes at Candidate Dredged-Material Disposal Sites B1B and 1M Offshore San Francisco

Volume 1: Analyses and Discussion

C. R. Sherwood   D. W. Denbo
D. A. Coats   J. P. Downing

October 1990

❀ Battelle

DISCLAIMER

Price Code	Page Range	Price Code	Page Range
A02	1- 10	A15	326-350
A03	11- 50	A16	351-375
A04	51- 75	A17	376-400
A05	76-100	A18	401-425
A06	101-125	A19	426-450
A07	126-150	A20	451-475
A08	151-175	A21	476-500
A09	176-200	A22	501-525
A10	201-225	A23	526-550
A11	226-250	A24	551-575
A12	251-275	A25	576-600
A13	276-300	A99	601-Up
A14	301-325		

PHYSICAL OCEANOGRAPHIC PROCESSES AT
CANDIDATE DREDGED-MATERIAL DISPOSAL
SITES B1B AND 1M
OFFSHORE SAN FRANCISCO

Volume 1: Analyses and Discussion

C. R. Sherwood
D. A. Coats[a]
D. W. Denbo
J. P. Downing

Battelle/Marine Sciences Laboratory
Sequim, Washington

October 1990

▲

(a) Marine Research Specialists
     3639 Harbour Boulevard, Suite 208
     Ventura, California 93001

PREFACE TO VOLUME 1

This is Volume 1 of a two-volume report that presents information gathered during a study of two candidate dredged-material disposal sites located offshore San Francisco. This volume provides project background, summary of methods, results, discussions, and conclusions; Volume 2 contains several appendixes that provide details of the data analyses and full presentations of data and results.

SUMMARY

The U.S. Army Corps of Engineers (USACE), San Francisco District, has identified two candidate sites for ocean disposal of material from several dredging projects in San Francisco Bay. The disposal site is to be designated under Section 103 of the Ocean Dumping Act. One of the specific criteria in the Ocean Dumping Act is that the physical environments of the candidate sites be considered. Toward this goal, the USACE requested that the Pacific Northwest Laboratory conduct a study of physical oceanographic and sediment transport processes at the candidate sites, B1B and 1M. The results of that study are presented in this report.

Site B1B is located approximately 12 nautical miles (nmi) offshore Half Moon Bay in water 86 m deep. Site 1M is closer to the Golden Gate, 12 nmi northwest of Point San Pedro, in water 42 m deep. The measurement program consisted of 4 deployments of subsurface moorings with current meters and optical suspended-sediment sensors over a 13-month period between April 1988 and May 1989. At Site B1B, the current meters were at depths of 21, 46, and 85 m, and the sediment sensor was 0.36 m above the bottom. At Site 1M, current meters were at depths of 21 and 40 m, and the sediment sensor was 0.36 m above the bottom. Data recovery was excellent, except for the loss of near-bottom current meter information during the final deployment at Site B1B and the loss of sediment sensor information during the final deployment at Site 1M. Wind data from National Data Buoy Center Buoy 46012 were obtained to assist in the interpretation of the current data, and wave data for use in sediment transport calculations were obtained from the Montara array, which is maintained by the Coastal Data Information Program.

Analysis of the current measurements indicates that, for the 13-month period, the mean alongshore component of currents was southward at both sites and all depths except at 21 m at Site 1M, where the alongshore mean was northward. Seasonal variations in the strength of the alongshore currents occurred at Site B1B, but flow was southward at all depths and in both spring/summer and fall/winter seasons. Seasonal reversals of flow occurred at Site 1M. In spring/summer, alongshore flow was southward near the bottom (40 m) and northward at 21 m. In fall/winter, the opposite occurred, and

mean flow was northward near the bottom and southward at 21 m. Low-frequency currents were mostly aligned with the regional bathymetric contours at both sites. Tides were predominantly cross-shelf at both sites. Tidal currents were stronger at Site 1M, and the semidiurnal M2 tidal ellipse was oriented toward the entrance of San Francisco Bay. Tides at Site B1B were weaker and more rotary in nature. Tidal currents accounted for approximately 50% of the variance in current velocity at Site B1B and about 70% of the variance at Site 1M. Wind-driven flows accounted for 40% to 50% of the variance in current velocities over periods of 2 to 10 days. Current patterns at both sites differed from the accepted continental shelf circulation pattern described by previous researchers. At Site B1B, the differences may be caused by year-to-year changes in the shelf current regime. In addition to year-to-year variability, the differences at Site 1M are likely due to the nearshore location in the Gulf of the Farallones.

Sediment-transport calculations were performed using a wave-current boundary layer model, measured current velocities, and wave parameters estimated from data recorded at Montara. The calculations predicted the vertical profiles for sediment concentration and velocity, and estimated rates and directions of suspended-sediment transport. The sediment transport calculations indicated that resuspension of bottom material at both sites is caused primarily by wave action and occurs much more frequently in fall/winter, when long-period swell from distant storms and shorter-period wind waves from intense local storms both cause higher wave-orbital velocities near the bottom. Resuspension occurs more frequently at the shallower Site 1M because more wave energy reaches the bottom. Primarily for this reason, calculated sediment transport rates at Site 1M are approximately 10 to 20 times higher than transport rates at Site B1B. In addition, because more energy reaches the bottom, material at Site 1M will be transported that would remain immobile at Site B1B. Calculated net transport at both sites is southward and offshore. At Site B1B, the mean transport direction corre-sponds closely with the mean current direction. At Site 1M, the timing of resuspension events causes the calculated mean sediment transport to diverge from the mean current direction, which has a substantial onshore component.

ACKNOWLEDGMENTS

CONTENTS

FIGURES

TABLES

1.0 INTRODUCTION

1.1 PROJECT BACKGROUND

The U.S. Army Corps of Engineers (USACE), San Francisco District, is in the process of identifying a suitable site for ocean disposal of material from several dredging projects in San Francisco Bay. Two candidate sites were selected by the USACE for detailed study. Site B1B (37°29'00"N, 122°48'00"W) is located approximately 12 nautical miles (nmi) west of Half Moon Bay, in water approximately 86 m (282 ft) deep, and Site 1M (38°38'42"N, 122°42'16"W) is located about 12 nmi northwest of Point San Pedro in water approximately 42 m (138 ft) deep (Figure 1.1). The USACE contracted with Pacific Northwest Laboratory[a] (PNL) to perform a study of physical oceanographic and sediment transport processes at the two candidate sites, and this report describes the results of that study.

The disposal site is to be designated under Section 103 of the Ocean Dumping Act with specific criteria set forth in 40 CFR 228.5-228.6. Included among these criteria is consideration of the physical environmental processes in and near the candidate sites. Of particular importance among physical considerations is dispersion of dredged material away from the candidate sites and especially transport of the material toward environmentally sensitive sites, such as the Point Reyes--Farallon Islands National Marine Sanctuary.

The objective of this study was to evaluate and compare the stability and eventual fate of dredged material placed at the two sites. To achieve this objective, measurements of currents, water temperature, and suspended sediments were made at the two sites during a 13-month period from April 1988 to May 1989. These data were augmented by wind and wave data obtained from established buoys and pressure gages. Sediment transport calculations were made using the wave, current, and suspended sediment data. In addition, statistical summaries of the measurements were generated, and an interpretive description of the physical processes important in the dispersion and

_____

(a) Pacific Northwest Laboratory is operated for the U.S. Department of Energy by Battelle Memorial Institute under Contract DE-AC06-76RLO 1830.
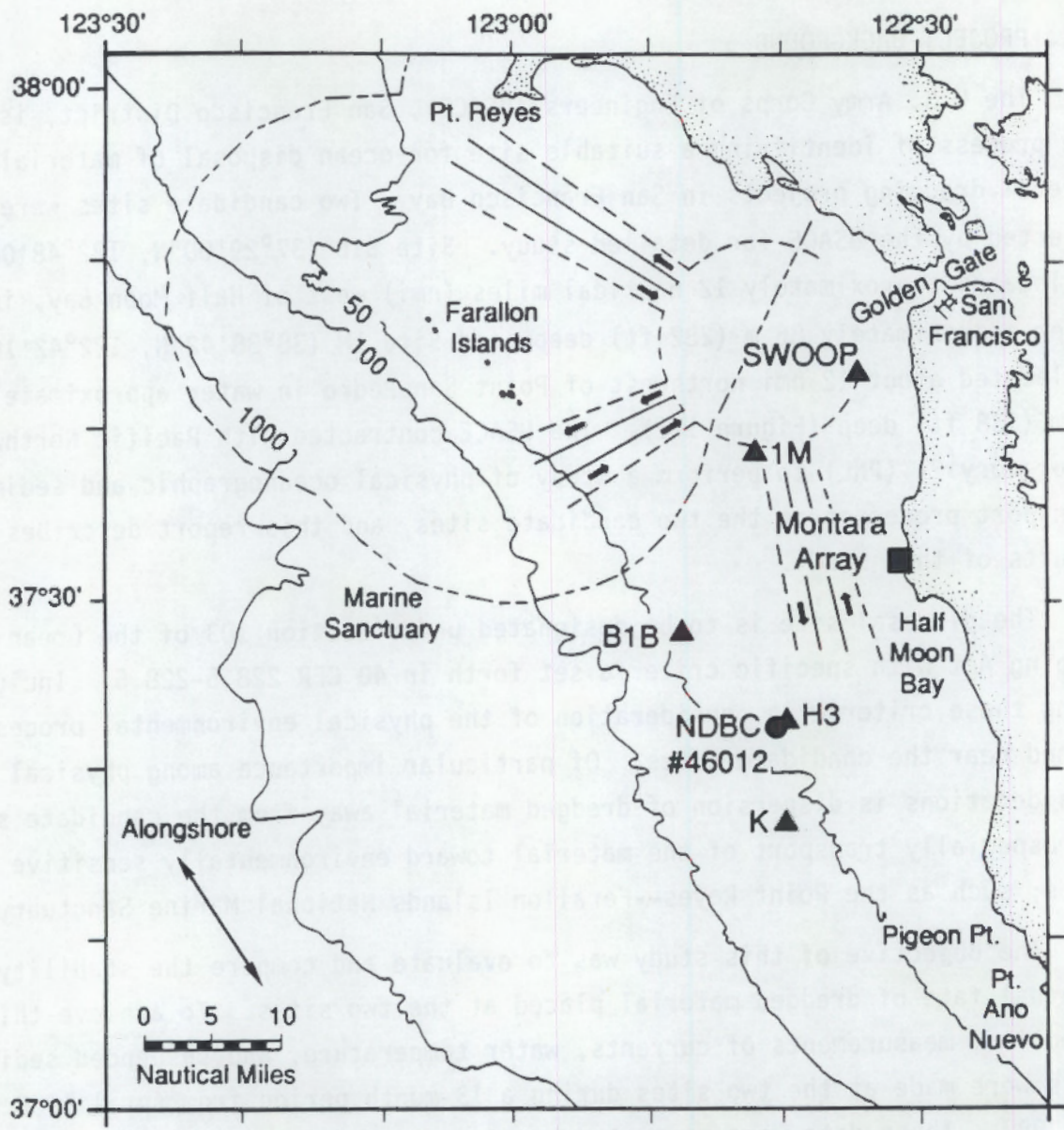
FIGURE 1.1. Map of the Study Area Showing Location of Candidate Disposal Sites B1B and 1M. Also shown are locations where wind (circle), wave (square), and current meter (triangles) data discussed in this report were collected.

transport of sediment was made. Finally, an analysis of the observed oceano-graphic climate was made to place the physical processes at the two sites in context with regional, long-term shelf circulation. This final activity is necessary to gage how well conclusions based on these 13-month measurements represent long-term mean and extreme conditions at Sites B1B and 1M.

1.2 STRUCTURE OF THIS REPORT

Volume 1 of this report is a summary of the important results and con-clusions from the study. Complete discussion of the measurement program, methods of data analysis, and extensive tabulation of results are presented in four appendixes located in Volume 2. In Volume 1 of this report, Section 1.0 presents background information including a review of the processes important in determining continental shelf circulation. Section 2.0 briefly summarizes the measurement program and lists other sources of data discussed in this report. In Section 3.0, the measurements of currents, water temperature, and suspended sediment are presented and discussed along with the wind and wave data obtained from other sources. Processes that control sediment transport are discussed, and calculated estimates of sediment transport at Sites B1B and 1M during the 13-month period are presented and interpreted. A discussion of the data from this measurement program and from other studies is presented in Section 4.0. The important conclusions from this study and the implications for dredged-material disposal are summarized in Section 5.0. References appear in Section 6.0.

Four appendixes are included in Volume 2 of this report. Appendix A is a report on a detailed bathymetric survey of Site B1B performed in May 1989. Appendix B contains details of the measurement program and data analysis as well as extensive graphic and tabular presentations of the data. Appendix C discusses the sediment transport calculations. Finally, Appendix D documents the computer tape containing current meter data from the measurement program.

1.3

1.3 REGIONAL OCEANOGRAPHY

1.3.1 The California Current System

Oceanographers have developed a detailed description of the California Current System (CCS) that will be summarized here (Chelton 1984; Hickey 1979; Huyer 1990; Lynn and Simpson 1987; Reid and Schwartzlose 1962). The main feature of the CCS (Figure 1.2) is the eastern limb of the North Pacific Gyre called the California Current (CC). The CC is a broad current that flows south[a] in a zone from 100 to 1000 km offshore and transports relatively fresh, cool water with a high oxygen content. The CC is more than 200 m deep, always flows south, and is strongest at the surface with typical speeds of 10 to 20 cm·s^{-1} that vary seasonally. Landward of the CC, the Davidson Current flows north over the outer continental shelf (50 m and deeper) and the continental slope. It also varies seasonally. During the fall/winter, the Davidson Current occupies the whole water column but is strongest at the surface. During spring/summer, upwelling produces a narrow southward current, called the upwelling jet, with highest velocities at the surface. This current is driven by density gradients caused by the upwelling front (Figure 1.3), and when it develops, southward flow overrides the Davidson Current at the surface. The spring/summer remnant of the Davidson Current flows northward near the bottom over the shelf-slope break. It is called the Poleward Undercurrent in the literature; however, for clarity, it will be called the Davidson Current in this report. Satellite and drifter observations indicate that strong episodic flows perpendicular to the coast, which Davis (1985) calls "squirts" and "jets," are superimposed on the CCS.

1.3.2 Shelf Processes

Currents on the California continental shelf generally flow parallel to the local depth contours and are driven by the large-scale, alongshore wind fields. The alongshore wind field is a good predictor of shelf circulation

---

(a) In this report, the terms "south," "southward," "north," and "northward" are used loosely to mean coast-parallel flow in the general direction indicated. These terms replace "poleward" and "equatorward," as used in the geophysical literature.

1.4
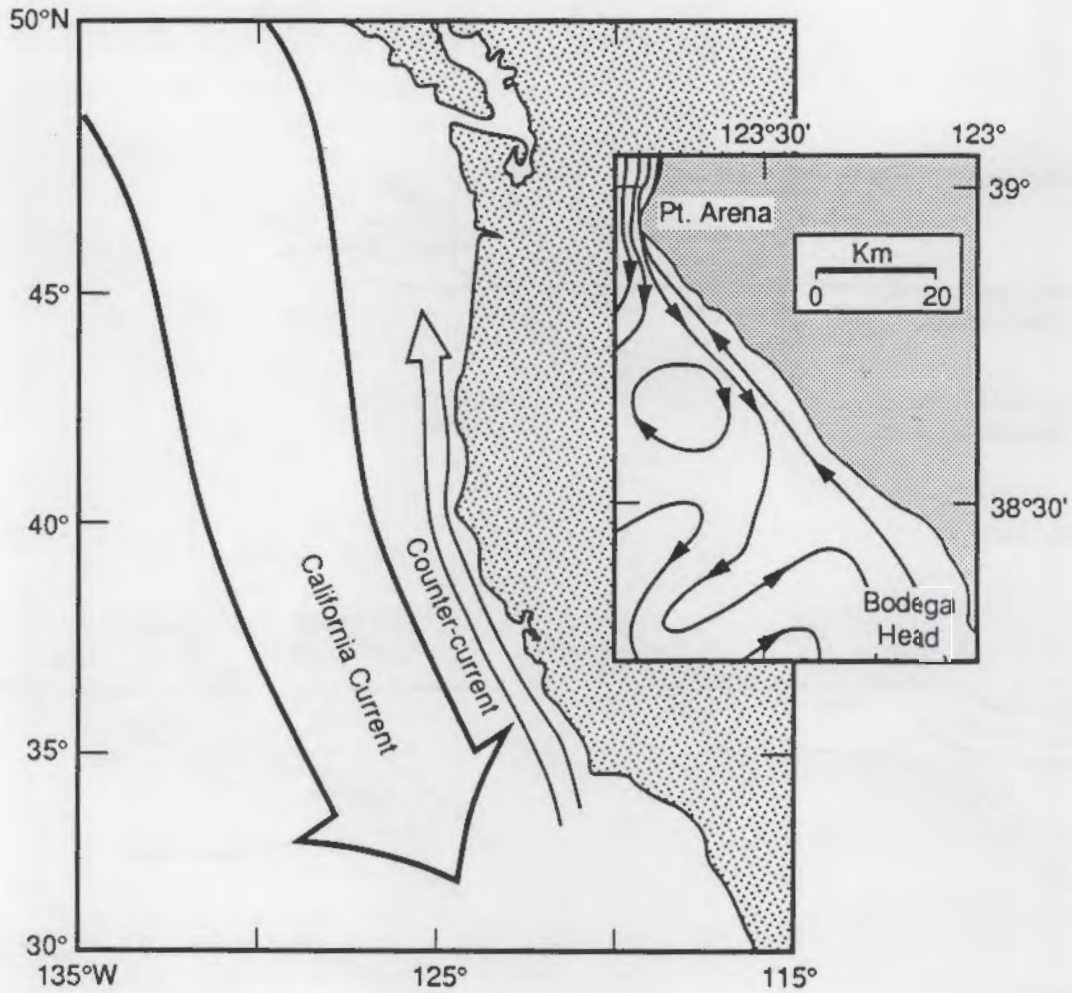
FIGURE 1.2. Illustration of the California Current System. Broad arrow is California Current; Davidson Current is open arrow nearshore. Inset shows surface current streamlines for an eddy and a meander around a jet (squirt).

when good wind information is available for about 1000 km of the coast (Denbo and Allen 1987). For the central California Shelf, the best predictor of alongshore, wind-driven currents is wind data from the region several hundred kilometers to the south.

1.5
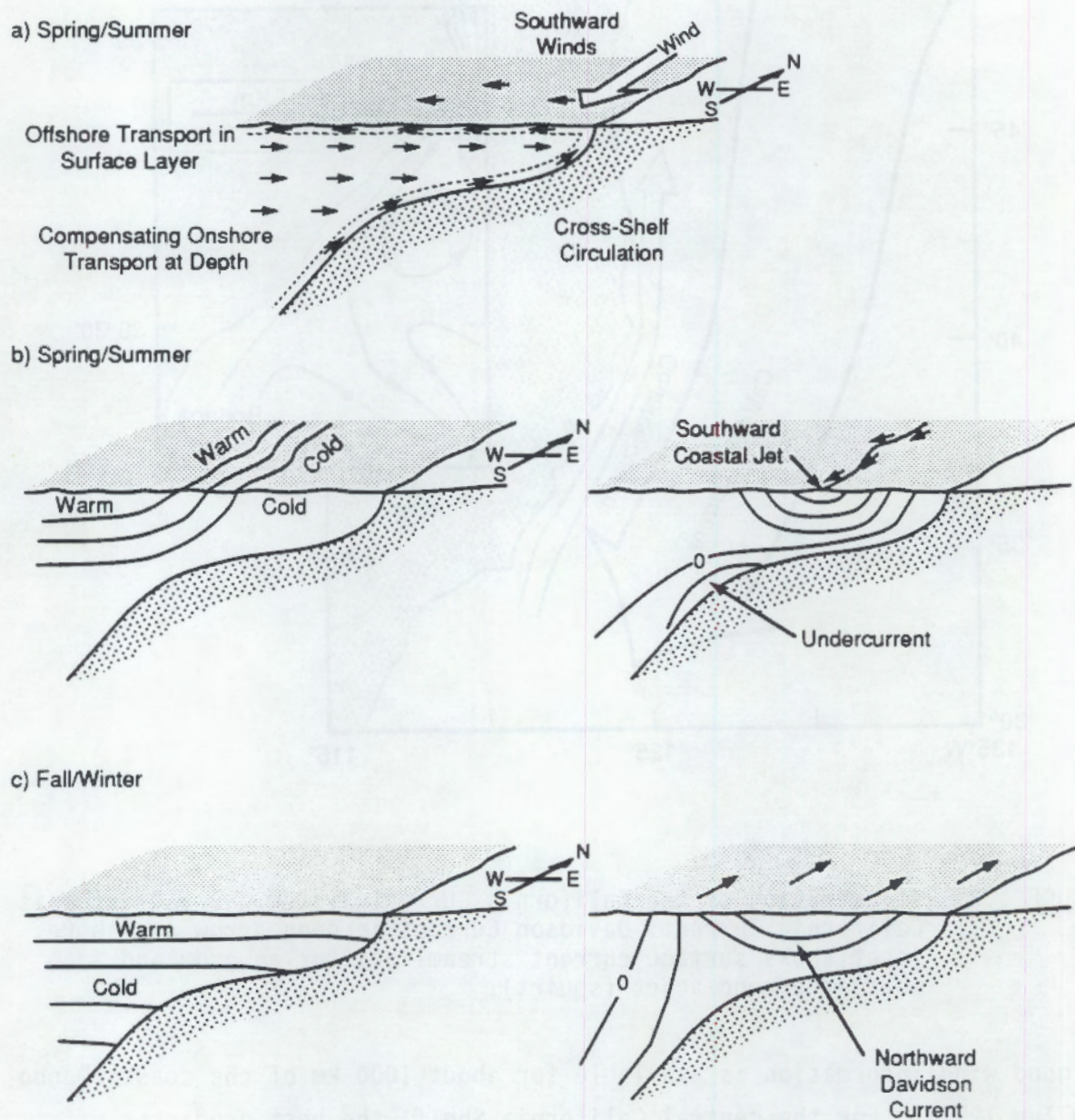
FIGURE 1.3. Illustration of Seasonal Characteristics of the California Current System. Top (upwelling cross-shelf circulation): southward, upwelling-favorable winds, and cross-shelf circulation. Middle (spring/summer): water temperature (density) and velocity distributions. Bottom (fall/winter): water temperature and velocity distributions.

1.6

Southward winds, in combination with the Coriolis effect of the earth's rotation, are particularly important because they cause upwelling (Figure 1.3). During upwelling events, the wind moves water offshore at the surface. This offshore transport is balanced by onshore transport of cold, nutrient-rich waters in the lower water column. The upwelling system of cross-shelf and vertical circulation combines with the wind to influence alongshore coastal currents. When the cold water rises to the surface, a front develops between warm water offshore and cold water upwelled near the coast. Density differences across the upwelling front create a pressure gradient that drives a current along the front. The current associated with this front has a southward jet located over the mid-shelf with maximum core velocities at the surface of about 25 $cm \cdot s^{-1}$. Freshwater runoff from large rivers can form a second front between upwelled salty water and brackish water very near the coast. This front, however, does not produce a strong surface current.

The wind- and density-driven currents vary slowly in response to changes in coastal weather patterns. Fluctuations in the wind- and density-driven shelf circulation occur over 2 to 7 days in response to both fast-moving winter storms and to longer-term changes in regional weather patterns. Fluctuations in current velocities are also caused by abrupt changes in the orientation of depth contours, which can produce eddies and strong flow perpendicular to the coast (squirts and jets). These flows may be responsible for transporting large amounts of water onto and off of the shelf. Observations of current-following drifters, made during the Coastal Ocean Dynamics Experiment (CODE) (Winant et al. 1987), show that eddies are about the same size as the width of the shelf. Fluctuations in currents caused by these eddies occur over periods of about 1 to 2 days. Fairly persistent eddies have been observed on the downstream sides of headlands and capes (e.g., off Point Reyes). Where eddies occur, current velocities tends to be higher and current directions more variable than on other parts of the shelf.

Tidal forces generate current fluctuations with periods of about 12 and 24 hours. These fluctuations have much lower amplitudes, about 10 to 15 $cm \cdot s^{-1}$, than the slowly varying circulation caused by the wind- and density-driven currents on which they are superimposed. At the CODE site, for

1.7

example, the tidal current energy in the summer was about one third that of the more slowly varying currents. Tidal current energy is estimated from the total variance of current speed in two narrow ranges of frequencies that include the diurnal (daily) and semidiurnal (twice-daily) tidal periods. Tidal currents increase near the entrance to large bays and estuaries, such as San Francisco Bay, as a result of the exchange of large volumes of water twice a day through narrow entrance channels.

1.3.3 Seasonal Variability and Annual Cycle

The coastal oceanographic seasons are regulated by large-scale wind fields. The two seasonal regimes are spring/summer, when the winds are southward and favor upwelling, and fall/winter, when the winds are more erratic and, on the average, northward or weakly southward. The length of the transition period between these seasonal regimes depends on the movement and location of a large, persistent high-pressure system called the North Pacific High. This system also controls the weather in the north Pacific and along the west coast of North America.

The large-scale coastal winds that influence coastal currents are divided into two major regimes. The northern regime, north of 37°N, has southward, upwelling-favorable winds during spring/summer and northward winds during fall/winter. The southern regime has southward winds throughout the year, which intensify during spring/summer. These wind regimes are regulated by the position of the North Pacific High. The North Pacific High strengthens and moves from a region centered at 28°N 130°W in February, to one near 38°N 150°W in August. A northward progression of maximum southward winds from 25°N in January to 38°N in July (Huyer 1983) accompanies the shift of the High. The exact timing of the seasonal change in wind patterns varies from year to year but, in this report, spring/summer is defined as the period from May 15 through September 30 and fall/winter as the period from November 1 through March 14. April and October are transitional months that may extend either season.

Spring/Summer

The transition to the spring/summer season occurs when the North Pacific High strengthens and moves north (Huyer 1983). Shelf waters along the coast

from Canada to Baja respond with an abrupt drop in mean sea level (about 10 cm) and cooler sea surface temperatures (Strub et al. 1987). The onset of these conditions usually occurs in March or April. Southward winds along the coast and upwelling (Huyer 1983) establish a front and a surface jet that combine with the Davidson Current to produce southward flow at the surface and northward flow at the bottom. As the season progresses, winds favorable to upwelling continue, the position of the upwelling front stabilizes, and offshore flow of surface water occurs (Winant et al. 1987). Landward of the front the upwelled waters are homogenous, and currents are constant from the surface to near the bottom. The southward wind occasionally weakens or reverses, in what are called "relaxation events," changing the balance of forces and allowing the front to move landward and sometimes disappear as upwelling weakens or shuts down completely. Vertical stratification of the inner shelf can be established during relaxation events by surface heating and the flow of warmer surface water from offshore.

Fall/Winter

The transition from spring/summer to fall/winter conditions occurs when the North Pacific High weakens and moves southeast. Its movement relaxes the upwelling-favorable winds and, north of 37°N, often allows them to reverse direction. With movement of the North Pacific High, storm tracks shift south, upwelling-favorable winds diminish, and the upwelling front moves landward and dissipates. Dissipation of the front and associated jet permits the Davidson Current to flow north at the surface. The transition to fall/winter usually begins when several storms pass through the region over a period of a few weeks.

1.3.4 Annual and Interannual Variability

The strength of upwelling-favorable winds and timing of the spring transition varies from year to year. Movement of the North Pacific High to the northwest and the onset of spring/summer usually occur in March or April (Strub et al. 1987). Large-scale changes during strong El Nino years can also affect the CCS (Huyer and Smith 1985). El Nino is an intermittent phenomena, best known for causing the upwelling system off South America to shut down, but also associated with shifts in the meteorologic and oceanographic systems

1.9

across the equatorial Pacific and in the North Pacific. During the 1982 El Nino, sea level along western North America rose about 20 cm above the mean, southward winds were weaker, and the coastal circulation was atypical in the summer. Specifically, upwelling transports were diminished, sea-surface temperatures were higher, and surface velocities in the coastal jet were weaker than normal.

Annual variability is also caused by changes in the strength and location of eddies, squirts, and jets. The presence or absence of them can dominate the mean current velocity on the shelf over periods of weeks to months. Thus, annual variations in the monthly mean current velocities can be caused by a combination of large-scale and local processes. For these reasons, long-term monthly mean directions can only be predicted confidently from several years of current data.

1.4 OCEANOGRAPHIC SETTING OFFSHORE SAN FRANCISCO

1.4.1 Site Descriptions

Candidate disposal Sites B1B and 1M are located southwest of San Francisco on a relatively wide (30- to 40-km) portion of the north-central California continental shelf in a gulf bounded by the Farallon Islands to the west, Point Reyes to the north, and Point Ano Nuevo to the south. Both sites are located several kilometers south and east of the eastern boundary of the Point Reyes--Farallon Islands National Marine Sanctuary. Site B1B is located approximately 12 nmi west of Half Moon Bay (see Figure 1.1); water depth at the mooring location is approximately 86 m. The bottom slopes gently to the west-southwest and appeared smooth in a recent detailed bathymetric survey (Volume 2, Appendix A). Grab samples indicate that the bottom sediment is well-sorted fine to very fine sand (mean grain diameter of approximately 0.15 mm). Site 1M is located approximately 12 nmi northwest of Point San Pedro; the approximate depth at the mooring location is 42 m. No detailed survey has been performed at Site 1M but charts indicate a smooth bottom. Grab samples show that the sediment size is similar to, but slightly finer than, sediment at Site B1B. Mean grain size at Site 1M is approximately 0.10 mm. Tides in the study area are mixed semidiurnal with a mean range of about 1.16 m (3.8 ft)(NOS 1987).

1.4.2 Existing Data

Major oceanographic research programs have been conducted north of Point Reyes at the Coastal Ocean Dynamics Experiment (CODE) site (Allen et al. 1983) and south of Point Ano Nuevo in the Central California Coastal Circulation Study (CCCCS) area (Chelton et al. 1988). Long-term, large-scale hydrographic measurements have been made along central and southern California by the California Cooperative Fisheries Investigation (CalCOFI). The northern limit of the CalCOFI data set includes the region offshore San Francisco. The Large-Scale West Coast Shelf Experiment (SuperCODE) (Denbo et al. 1984) included synoptic measurements from current meters on the outer shelf and continental slope between 34°N and 43°N, including sites to the north and south of the Gulf of the Farallones (Denbo and Allen 1987). These studies have all provided information on the large-scale patterns and seasonal variability of circulation along the California coast and some detailed descriptions of important physical oceanographic processes (e.g., CODE), but none of them have focused on the circulation in the Gulf of the Farallones.

Current measurements made near Site B1B include mooring K of the CCCCS study, discussed in Chelton et al. (1988), and SuperCODE mooring H3 discussed in Denbo and Allen (1987). Current measurements made near Site 1M include those obtained during the design phase of the Southwest Ocean Outfall Project (SWOOP)(CH2M Hill et al. 1989; Roberts 1980) and recent measurements made to study diffusion in the outfall region.[a] Hydrographic measurements were also obtained during the SWOOP studies. The U.S. Geological Survey recently measured currents for 5 months at two other sites in the Gulf of the Farallones, (Noble and Gelfenbaum 1990) and the results of an extensive bottom-sediment study performed by the U.S. Geological Survey are in preparation.[b]

1.4.3 Local Circulation

There is evidence that the circulation in the Gulf of the Farallones is markedly different from the better-studied regions to the north and south. In

---

(a) P. J. W. Roberts, Georgia Institute of Technology, personal communication to D. W. Denbo, Pacific Northwest Laboratory, January 29, 1990.
(b) H. Karl, U.S. Geological Survey, personal communication to C. R. Sherwood, Pacific Northwest Laboratory, June 6, 1990.

addition to differences associated with the wide continental shelf and complicated topography, the region offshore of San Francisco is in a transition zone between a northern wind regime, which extends north from about $37°N$, and a southern regime (Halliwell and Allen 1987). The response to wind forcing during the spring transition is weaker in the southern regime and does not appear at all in some years. Sites B1B and 1M may be located in either regime, depending on the particular year. In 1981, for example, the northern regime extended south to include both sites while, in 1982, the southern regime moved north over the sites. This is known from sea level and wind measurements made during the SuperCODE experiment (Denbo and Allen 1987). The response of the coastal current to the wind is also different in the two years, and sea level at San Francisco was not as well correlated with the wind in 1981 as in 1982. Although upwelling does occur offshore of San Francisco, it is much weaker than in coastal areas to the north and south (Huyer 1983).

Long-term records from mooring K (16 nmi from Site B1B) indicate that currents flow southward from mid-February to mid-May, becoming more variable in spring and summer. Current data from a mooring south of mooring K showed mean northward flow at 70-m depths between Point Sur and Point Conception (Chelton et al. 1988).

Currents at Site 1M are likely to be influenced by tidal exchange through the Golden Gate and estuarine circulation caused by the discharge of brackish surface water from San Francisco Bay. Studies at NOS and SWOOP current meter moorings indicate that tidal currents are dominated by exchange through the entrance to San Francisco Bay, but that entrance effects generally decrease with radial distance from the Golden Gate (Roberts 1980; Tetra Tech Inc. 1987). Recent measurements near the SWDOP diffuser provide some evidence of estuarine circulation (e.g., net flow away from the entrance near the surface and net flow toward the entrance near the bottom).[a]

(a) P. J. W. Roberts, Georgia Institute of Technology, personal communication to D. W. Denbo, Pacific Northwest Laboratory, January 29, 1990.

1.4.4 Wave Climate

The USACE sponsors the Coastal Data Information Program (CDIP), which has monitored wave climate at many sites along the West Coast since 1978 with surface-following buoys, called waveriders, and bottom-mounted pressure gages. Both wave-measuring techniques produce a time series of sea-surface elevation from which wave statistics and oscillatory water motion near the bottom can be calculated. In addition to sea surface elevations, multiple bottom-pressure gages can provide information about the direction of wave travel. Waverider data, however, cannot provide such information.

Wave data have been collected intermittently with a waverider buoy near the Farallon Islands since 1982 and with a bottom-mounted array of pressure gages in 15 m of water near Montara (Figure 1.1). The wave height statistics from the Farallon Island location, for which the longest record is available, have been compiled to investigate the general wave climate, the seasonal cycle, and year-to-year variability in wave conditions representative of Sites B1B and 1M. Figure 1.4 summarizes the seasonal distribution of wave height probability-of-exceeding statistics for wave records from the Farallon Island buoy (1982 to 1987). The horizontal bars on Figure 1.4 indicate the percentage of time that significant wave heights exceeded the value shown on each bar. Significant wave height is estimated from wave records as 4σ, where σ is the standard deviation of sea surface elevation measured by a pressure gage or buoy. The heavy bars are the mean frequency that specific wave heights were exceeded, and the light bars indicate the ranges minimum and maximum frequency that those wave heights were exceeded. For example, in the most extreme winter recorded, wave heights exceeded 3 m 39% of the time. In the same period, waves were higher than 2 m 78% of the time.

Wave heights at the Farallon Island buoy usually exceed 3 m about 22% of the time in winter, but, during spring and summer, waves are higher than 3 m only about 4% of the time. Although 1987 is the only year for which wave statistics are available from both Farallon Island and Montara, the data from this year indicate that wave heights are lower at Montara. This could result from spreading (refraction) and dissipation of wave energy at the bottom as

1.13
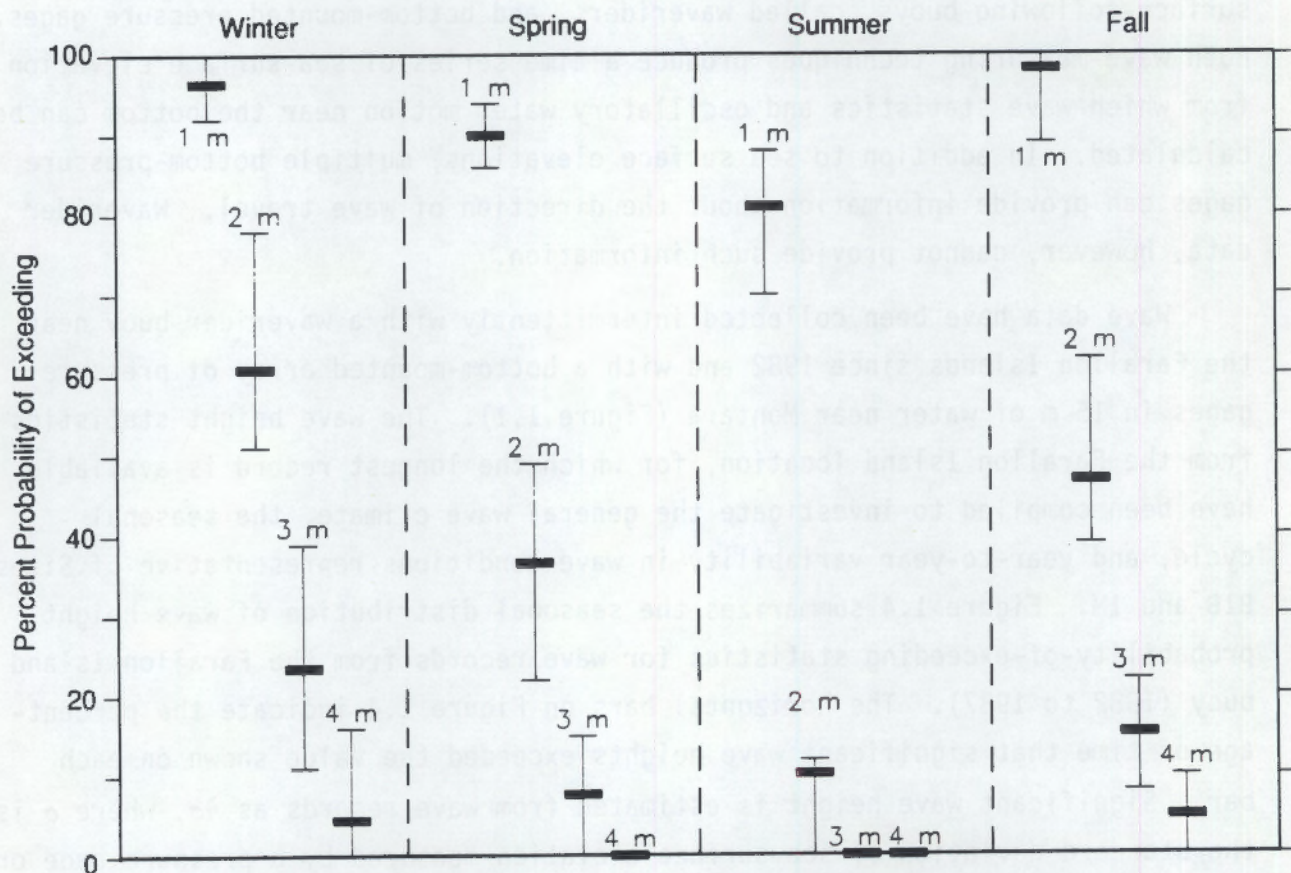
FIGURE 1.4. Summary of Seasonal Distribution of Wave-Height Probability-of-Exceeding Statistics, Farallon Island Buoy. Mean probability-of-exceeding certain heights for 1982-1987 is shown by heavy bar, extremes by lighter bars. Seasons are 3-month periods; winter is January, February, and March. Data are from CDIP (1988) and earlier reports.

waves cross the continental shelf. However, to draw any conclusions about the differences between the wave climates at the two observation sites, a longer common record is required.

Wave height information alone is not sufficient for predicting sediment transport because of the dependence of wave-orbital velocity on wave period and water depth. Table 1.1 illustrates the influence of these factors by showing the theoretical wave-orbital velocities of 3-m waves with different

1.14

TABLE 1.1. Near-Bottom Wave-Orbital Velocities ($cm \cdot s^{-1}$) for Linear Waves with 3-m Height and Periods from 6 to 20 s[a]

Depth, m	Wave Period, s							
	6	8	10	12	14	16	18	20
40	4	19	35	46	54	58	62	64
50	1	10	24	36	43	49	52	55
60	0	5	16	27	36	41	45	48
70	0	3	11	21	29	35	40	43
80	0	2	7	16	24	30	35	38
90	0	1	5	12	20	26	31	34
100	0	0	3	9	16	23	27	31
120	0	0	2	5	11	17	22	26
150	0	0	0	2	6	11	15	19

(a) From Komar (1976).

periods for a range of water depths. During winter, the frequency of occurrence of long-period waves (swell) increases at Farallon Island and Montara. Winter swell is mainly generated by storms in the northeast Pacific. Waves with dominant periods up to 25 s have been recorded by buoys off the northern California coast. During an extreme event in 1983, a 25-s swell with significant height of 11 m was recorded by a National Oceanic and Atmospheric Administration buoy (Earle et al. 1984). Waves with these heights and periods are capable of producing wave-orbital velocities of about 1.5 $m \cdot s^{-1}$ near the bottom at Site B1B. As will be shown in Section 3.0, the longer-period swells that occur in winter are very important factors in the assessment of sediment transport at Sites B1B and 1M. Seas generated on the continental shelf and the adjacent offshore waters by local storms have shorter periods (5 to 10 s). Seas generally produce lower near-bottom wave-orbital velocities than swell for a particular wave height and water depth. For example, a 3-m wave with an 8-s period will produce an orbital velocity of less than 2 $cm \cdot s^{-1}$ at Site B1B, whereas a 3-m wave with a 20-s period will produce an orbital velocity of about 36 $cm \cdot s^{-1}$ at the same location (Table 1.1). Because the local sea conditions and wind-driven currents may not be a good indicator of near-bottom orbital velocities from swell generated by a distant storm, it is important to account for longer-period swells when calculating near-bottom wave-orbital velocities. These factors are discussed in more detail in Volume 2, Appendix C.

2.0 MEASUREMENTS

The objective of the measurement program was to obtain site-specific current and suspended-sediment data 1) for physical characterization of the sites, and 2) for use as input in sediment transport calculations. Sections 2.1 and 2.2 provide a brief description of the measurement program and data recovered; a more complete description is provided in Volume 2, Appendix B. Wave and wind data from other sources were acquired to aid in the interpretation and for sediment transport calculations. These data are briefly described in Section 2.3.

2.1 MOORINGS AND INSTRUMENTS

The measurement program consisted of four deployments of moorings with current meters and optical suspended sediment sensors over a 13-month period between April 1988 and May 1989. The instruments and moorings were maintained by Kinetics Laboratories, Inc. (KLI) of Santa Cruz, California, under the supervision of Battelle, Ocean Sciences Division, Ventura Operations, of Ventura, California, and, later, under the supervision of Marine Research Specialists, Inc. (MRS), also of Ventura, California. Two moorings were maintained from April 1988 to May 1989, one located near the edge of candidate disposal Site B1B and one at Site 1M (Figure 1.1). The moorings were deployed four times and produced a data set containing nearly 13 months of temperature and current data from five current meters. Mooring configurations are shown in Figure 2.1. At Site B1B (water depth 86 m), current meters were moored at 21, 46, and 85 m and the suspended sediment sensor was mounted 0.36 m above the bottom. At Site 1M (water depth 42 m), the meter depths were 21 and 40 m, and the sediment sensor was mounted 0.36 m above the bottom.

Neil Brown Smart Acoustic Current Meters® (SACMs) were used to make the velocity measurements. The SACM is a true vector-averaging system and averaged the current over a 15-min sampling interval. On the final deployment

---

® Neil Brown Smart Acoustic Current Meter is a registered tradename of Neil Brown Instrument Systems, Cataumet, Massachusetts.

a) Site B1B

21 m — SACM

— Release

46 m — SACM

85 m — SACM

Depth   — Release   OBS   1.42 m
86 m   0.36 m

600' Groundline

b) Site 1M

21 m — SACM

40 m — SACM

Depth   — Release   OBS   1.56 m
42 m   0.36 m

600' Groundline
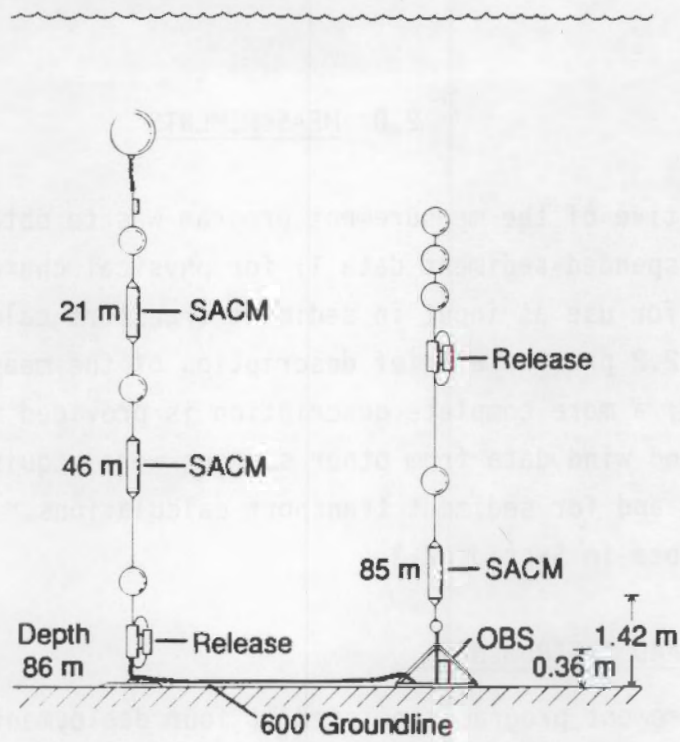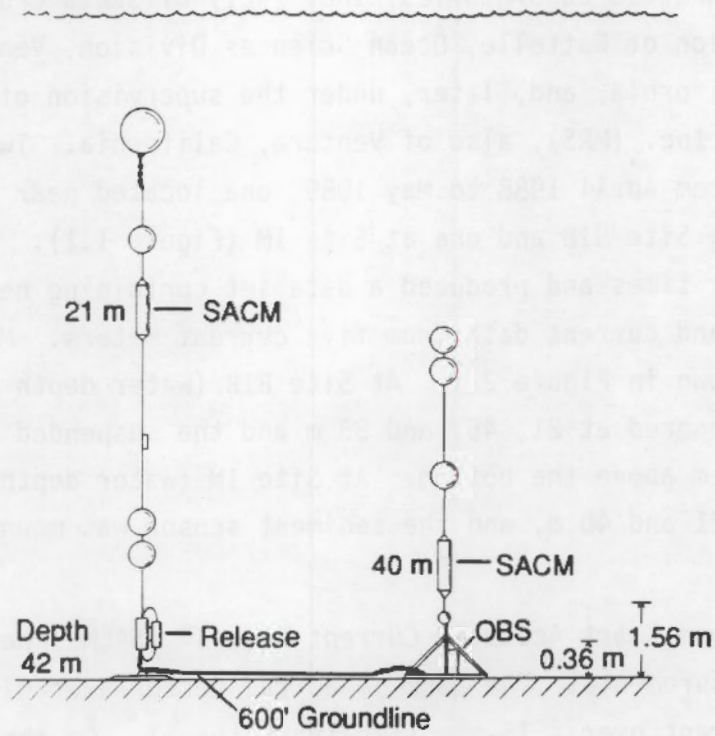
FIGURE 2.1. Configuration of Moorings Deployed at Sites B1B and 1M

at Site B1B, a Sea Data® Model 621 Directional Wave Current Meter (DWCM) was substituted for the SACM on the near-bottom mooring. The intent was to obtain direct measurements of the near-bottom wave-orbital velocities, but the instrument failed and only one component (direction unknown) of current data was acquired. Suspended sediment data were acquired using D&A Instruments optical backscatter (OBS®) sensors (Downing 1983). OBS sensors detect suspended particles by sensing infrared light scattered from them. The OBS circuit boards were housed in an Aanderaa® pressure case with batteries and a Campbell Scientific CR-10® programmable datalogger. The OBS sensors were programmed to warm up for 2 s and then measure 20 samples at 1 Hz every 15 min synchronously with the current meters. All 20 samples were stored when a predetermined OBS response threshold was exceeded; otherwise, the mean of the samples was stored. The sensors were calibrated with sediment obtained in grab samples from Sites B1B and 1M in the University of Washington calibration tank (Downing and Beach 1989).

2.2 DATA RECOVERY

The success of the field operations is measured by the excellent data recovery record, summarized in Table 2.1. There were, however, some noteworthy logistical and instrumentation problems. These are summarized below.

- Seventy-seven days of OBS sensor data, about 10% of a possible 767 days, were not recovered either because the CR-10 logger overwrote early records when its memory capacity was exceeded during long deployments or when the lithium batteries failed. Biofouling by barnacles during the third deployment was extensive and nearly made the sensor inoperable.

- Seven days of current meter data (1%) were not recorded because the SACM storage capacity was exceeded during the third deployment. No data were acquired from the near-bottom instrument during the fourth deployment at Site B1B because the DWCM failed.

® Sea Data Model 621 is a registered tradename of the Pacer Systems Company, Newton, Massachusetts.
® Aanderaa is a registered tradename of Aanderaa Instruments, Bergen, Norway.
® OBS is a registered trademark of D&A Instruments, Port Townsend, Washington.
® CR-10 is a registered tradename of Campbell Scientific, Inc., Logan, Utah.

TABLE 2.1. Summary of Current Meter and Suspended Sediment Measurement Program

Site	Location	Water Depth, m	Deployment/ Recovery	Instrument Depth/Height	Sample Rate	Data Interval, GMT Days	Comments
B1B	37°28'05.5"N 122°47'09.2"W	86	2001 PDT 4/26/88 1431 PDT 6/ 7/88	SACM(a,b) 21 m SACM 46 m SACM 85 m/1.42 m OBS(c) 86 m/0.36 m	300 s at 2 Hz; 15 min 300 s at 2 Hz; 15 min 300 s at 2 Hz; 15 min 10 s at 2 Hz; 15 min	118 - 159 118 - 159 118 - 159 118 - 159	
B1B	37°28'13.2"N 122°47'03.1"W	86	1712 PDT 6/ 8/88 1150 PDT 9/13/88	SACM 21 m SACM 46 m SACM 85 m/1.42 m OBS 86 m/0.36 m	300 s at 2 Hz; 15 min 300 s at 2 Hz; 15 min 300 s at 2 Hz; 15 min 10 s at 2 Hz; 15 min	162 - 245 162 - 245 162 - 258 183 - 258	Mooring probably released during unsuccessful recovery attempt on 9/1/88.
B1B	37°28'14.7"N 122°46'43.2"W	86	1118 PDT 9/15/88 1300 PST 1/20/89	SACM 21 m SACM 46 m SACM 85 m/1.42 m OBS 86 m/0.36 m	300 s at 2 Hz; 15 min 300 s at 2 Hz; 15 min 300 s at 2 Hz; 15 min 10 s at 2 Hz; 15 min	260 - 20 260 - 20 260 - 20 287 - 20	Beginning of data from OBS and bottom current meter overwritten. Standard deviation of OBS also recorded.
B1B	37°28'13.2"N 122°47'03.1"W	86	0900 PST 1/30/89 1420 PST 6/2/89	SACM 21 m SACM 46 m DWCM(d) 85 m/1.42 m OBS 86 m/0.36 m	300 s at 2 Hz; 15 min 300 s at 2 Hz; 15 min 10 s at 2 Hz; 15 min 10 s at 2 Hz; 15 min	31 - 153 31 - 153 none 31 - 153	Bottom current meter replaced with DWCM, only one velocity component recorded. 512 s OBS and velocity bursts every 4 h.
1M	37°38'49.8"N 122°42'01.3"W	42	1704 PDT 4/27/88 1203 PDT 6/ 7/88	SACM 21 m SACM 40 m/1.56 m OBS 42 m/0.36 m	300 s at 2 Hz; 15 min 300 s at 2 Hz; 15 min 10 s at 2 Hz; 15 min	129 - 159 129 - 159 129 - 159	Evidence of resuspension (silt) on mooring.
1M	37°38'42.6"N 122°42'16.0"W	42	1200 PDT 6 /9/88 0858 PDT 9/ 1/88	SACM 21 m SACM 40 m/1.56 m OBS 42 m/0.36 m	300 s at 2 Hz; 15 min 300 s at 2 Hz; 15 min 10 s at 2 Hz; 15 min	162 - 245 162 - 258 171 - 245	No evidence of resuspension on mooring.
1M	37°38'38.8"N 122°42'19.0"W	42	1317 PDT 9/2/88 1110 PST 1/21/89 & 1210 PST 1/30/89	SACM 21 m SACM 40 m/1.56 m OBS 42 m/0.36 m	300 s at 2 Hz; 15 min 300 s at 2 Hz; 15 min 10 s at 2 Hz; 15 min	247 - 17 247 - 17 257 - 30	Bottom current meter and OBS recovered 9 days later. Bottom mount and anchor settled in mud.

TABLE 2.1. (contd)

Site	Location	Water Depth, m	Deployment/ Recovery	Instrument Depth/Height	Sample Rate	Data Interval, GMT Days	Comments
1M	37°38'42.6"N	42	1300 PST 1/30/89	SACM 21 m	300 s at 2 Hz; 15 min	31 - 153	OBS battery failed.
	122°42'16.0"W		1703 PDT 6/02/89	SACM 40 m/1.56 m	300 s at 2 Hz; 15 min	31 - 153	
				OBS 42 m/0.36 m	10 s at 2 Hz; 15 min	none	

(a) Neil Brown Smart Acoustic Current Meter with temperature sensor.

(b) Use of trade names is for descriptive purposes only and is not endorsement of products by the U.S. Government.

(c) Optical Backscatterance Sensor (OBS), D&A Instruments.

(d) Sea Data 621 Directional Wave Current Meter.

- Gaps in the processed data resulting from a variety of other difficulties constitute 15% of the record for Site B1B and 4.5% of the record for Site 1M.

- Bad weather, acoustic release problems, and problems with deck equipment during recovery of moorings resulted in schedule disruptions totalling about 17 days.

- The Site B1B mooring was released on September 1, 1988, during the third deployment, but not recovered until September 13. During this time, the vertical position of the upper current meters was not known, and sediment resuspended by motion of the groundline or dragging of the mooring anchor dominated the OBS records.

Considering the fishing effort in this region, and based on prior experience with moored equipment in Alaska and Washington, this was a very successful field program.

2.3 WIND AND WAVE DATA

Digital wind data were acquired from National Data Buoy Center (NDBC) Buoy 46012 to aid in interpretation of the current meter data. The data, obtained from the National Oceanographic Data Center (NODC) covered the entire 13-month study period except for about 40 days in early 1989 when the anemometer was not operational. The data were adjusted to a standard elevation above sea level and used to estimate wind stress, as described in Volume 2, Appendix B.

Wave data recorded at the Montara array, located in 15-m water depth, were obtained in digital form from the Coastal Data Information Program (CDIP) (Seymour et al. 1985) for use in sediment transport calculations. Wave spectral density in nine frequency bands were provided for every 4 to 6 h over the entire study period. Also provided were calculated significant heights and periods. The processing of the wave data is described in Volume 2, Appendixes B and C.

3.0 RESULTS

3.1 OCEANOGRAPHIC DATA

3.1.1 Time Series

Time-series plots of the current and wind data provide an overview of the measurements made during this study. Vector plots of the low-frequency currents measured at Sites B1B and 1M are shown in Figures 3.1 and 3.2. In these plots, the data have been filtered with a 40-h low-pass filter that effectively removes tidal currents and retains wind-driven flows and other low-frequency phenomena. The current velocity vectors are represented as sticks with a length corresponding to the flow speed and are plotted at 6-h intervals. The sticks point in the direction toward which the current was flowing; alongshore (328°T in this report) is toward the top of the page and onshore is toward the right. Wind data from NDBC Buoy 46012 (also smoothed with a 40-h low-pass filter) are plotted using the same format in the top panel of both figures. The alongshore components of the 40-h low-pass filtered data from both sites are plotted in Figures 3.3 and 3.4. These plots show only the component of the low-frequency flow parallel to the regional depth contours (northward is toward the top of the page). Plots of the cross-shelf component and detailed discussion of the data processing are provided in Appendix B. Temperatures measured at the two sites are plotted in Figure 3.5; these have also been smoothed with a 40-h low pass filter to remove fluctuations caused by tides and other short-period phenomena.

The time-series plots (Figures 3.1 to 3.5) emphasize seasonal changes at the two sites and will be discussed in chronological fashion. The initial deployments were made in late April when southward winds predominated. Southward and offshore flows occurred at the upper instruments at both moorings, and water temperatures dropped rapidly at the beginning of the study period, suggesting that upwelling was occurring. Water temperature differences between the mid-depth and bottom instruments at Site B1B decreased, indicating a decrease in the stratification of the bottom waters. Strong southward flows with a weak offshore component were measured at the upper (21-m) instrument at Site B1B, and although currents at the two deeper

3.1
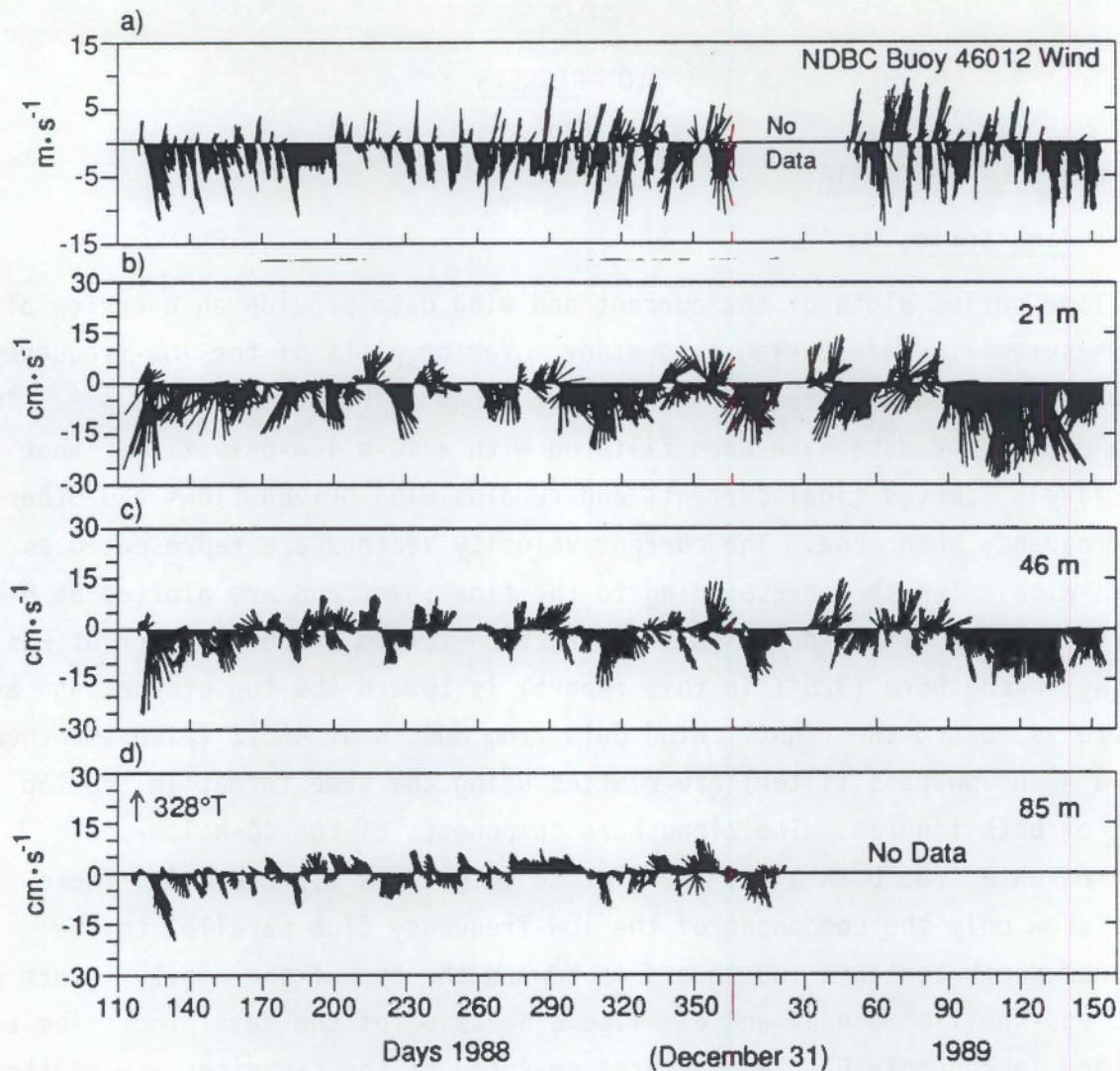
FIGURE 3.1. Vector Plots of 40-h Low-Pass Filtered Winds at NDBC Buoy
46012 and Currents at Depths of 21 m, 46 m, and 85 m,
Site B1B

meters showed similar fluctuations in alongshore speed, currents at Site B1B
generally decreased and rotated shoreward with depth. Only small temperature
differences were measured between the two instruments at Site 1M, also indi-
cating that the water column was weakly stratified. A strong, persistent
pulse of southward flow was recorded at Site 1M during this period (days 150
to 190); this event is one of the largest transport events of the measurement
program and is anomalous because there is no evidence for these strong
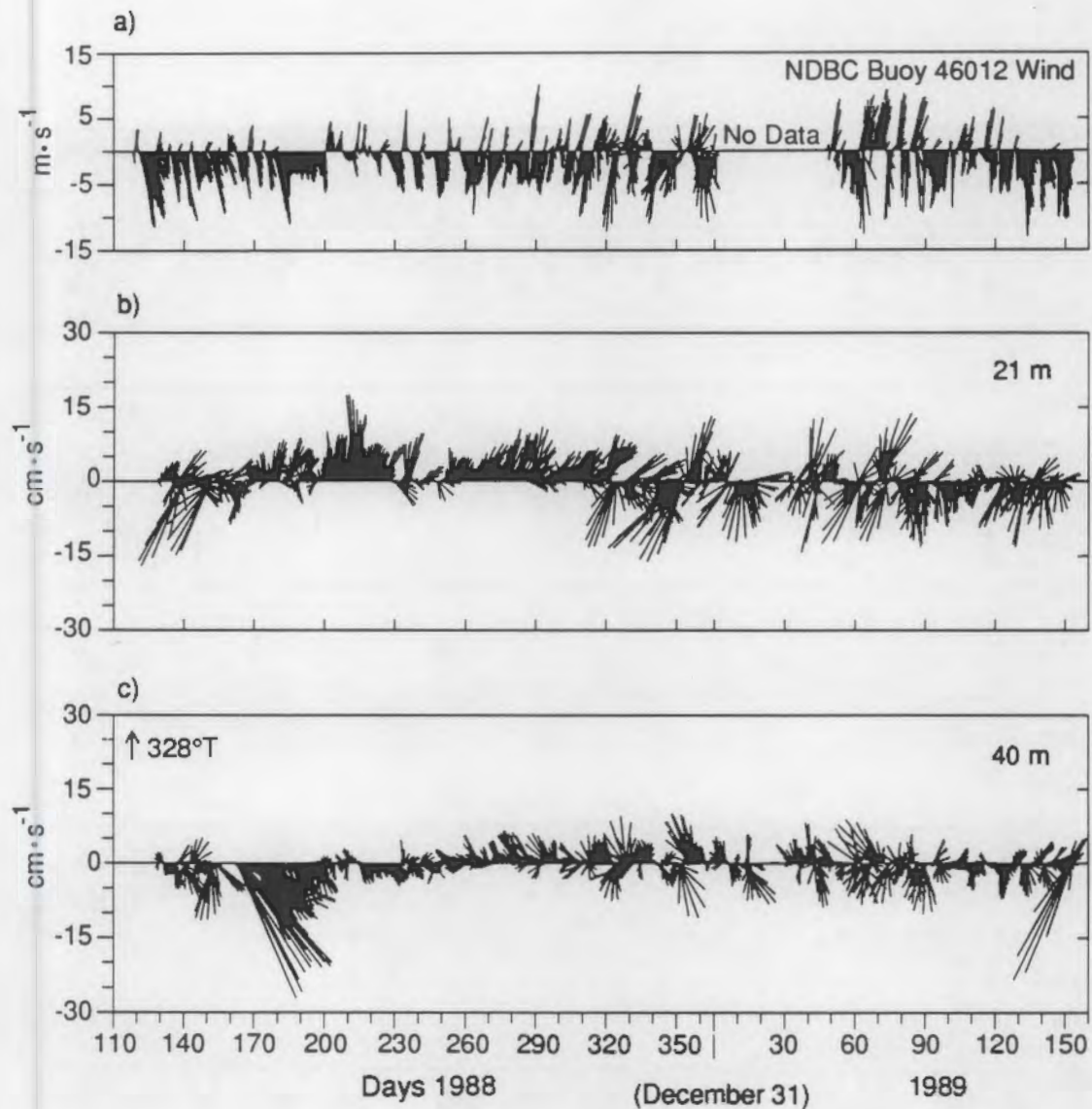
FIGURE 3.2. Vector Plots of 40-h Low-Pass Filtered Winds at NDBC Buoy 46012 and Currents at Depths of 21 m and 40 m, Site 1M

currents at the 21-m instrument. Significant wave heights measured at the Montara array during this period varied, occasionally reaching 2.5 m (Figure 3.6).

The southward winds slowed and reversed during a relaxation event that began on July 18 (day 200). After this date, southward winds were less persistent, and strong northward flows occurred at the shallow (21-m) Site 1M instrument. Water temperatures rose at all instruments, and temperature
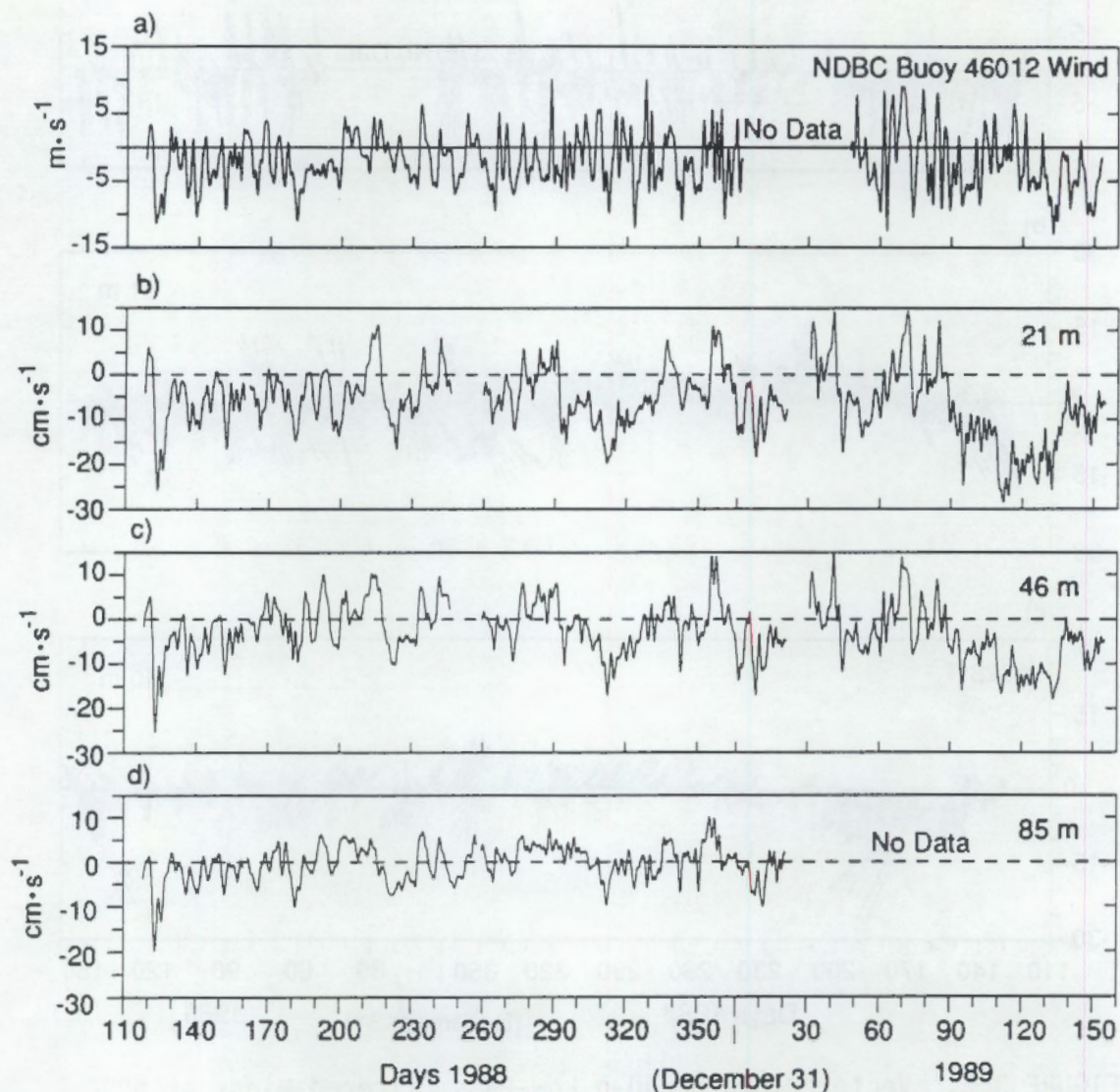
FIGURE 3.3.   Time Series of Alongshore Component of 40-h Low-Pass Filtered
              Winds at NDCB Buoy 46012 and Currents at Depths of 21 m, 46 m,
              and 85 m, Site B1B

differences between depths increased. These changes suggest that the
upwelling system shut down, and the rapid temperature rise, in conjunction
with the northward flow, suggests that warm water may have been advected to
the study area from the south. Alongshore flows at most instruments were
variable during the remainder of the summer except at the 21-m instrument at
Site 1M, where they were persistently northward and onshore. Some long

3.4

a)

15
5
-5
-15
m·s⁻¹

NDBC Buoy 46012 Wind

No Data

b)

20
10
0
-10
-20
cm·s⁻¹

21 m

c)

10
0
-10
-20
-30
cm·s⁻¹

40 m

110 140 170 200 230 260 290 320 350 | 30 60 90 120 150

Days 1988   (December 31)   1989
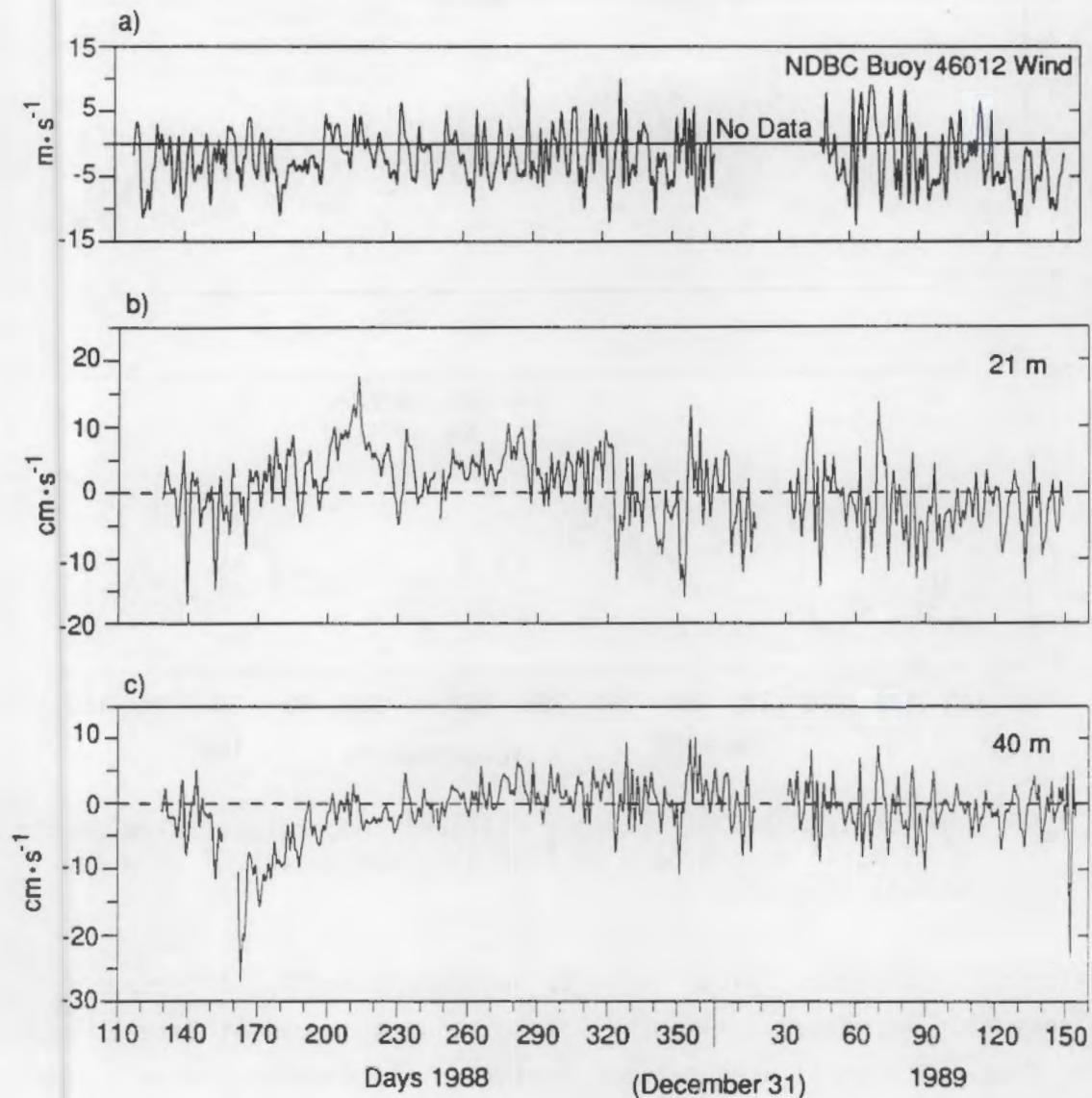
FIGURE 3.4.   Time Series of Alongshore Component of 40-h Low-Pass Filtered
Winds at NDCB Buoy 46012 and Currents at Depths of 21 m and
40 m, Site 1M

periods of net southward flow at Site B1B were recorded. Waves were smaller,
with significant heights generally less than 1.5 m during the period.

The onset of the winter-storm season on about November 5 (day 310) is
best marked by an increase in wave heights (Figure 3.6). After this date,
significant wave heights frequently exceeded 2 m and often reached 3 m.
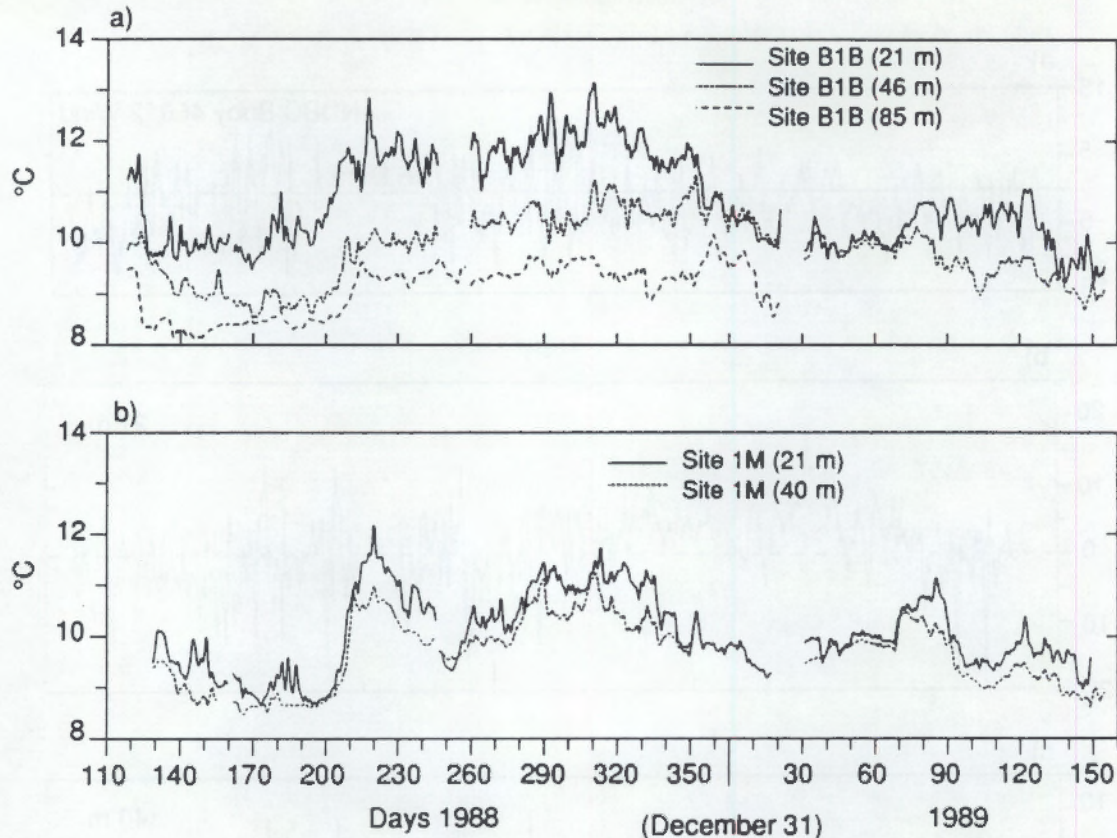
FIGURE 3.5. Time Series of 40-h Low-Pass Filtered Temperatures from Depths of 21 m, 46 m, and 85 m at Site B1B, and Depths of 21 m and 40 m at Site 1M

Temperatures in the water column began to decrease steadily, and current speeds generally increased. Alongshore low-frequency flows at Site 1M and winds at Buoy 46012 oscillated between northward and southward with larger amplitude than during summer. Temperature differences between the upper instruments at Site B1B and the two Site 1M instruments became very small, suggesting cooling and mixing of the water column. The wave data indicate that a large storm occurred on about December 21 (day 356), when wave heights reached 4.18 m, the highest of the study period. Strong northward flows associated with this event were recorded at the 21-m instruments at both sites. A second high-wave event occurred on December 31. Waves remained generally higher than in the summer for the remainder of the winter season, but no notable storms occurred in early 1989.

3.6

a) Significant Wave Height

b) Dominant Period

Days 1988   (December 31)   1989
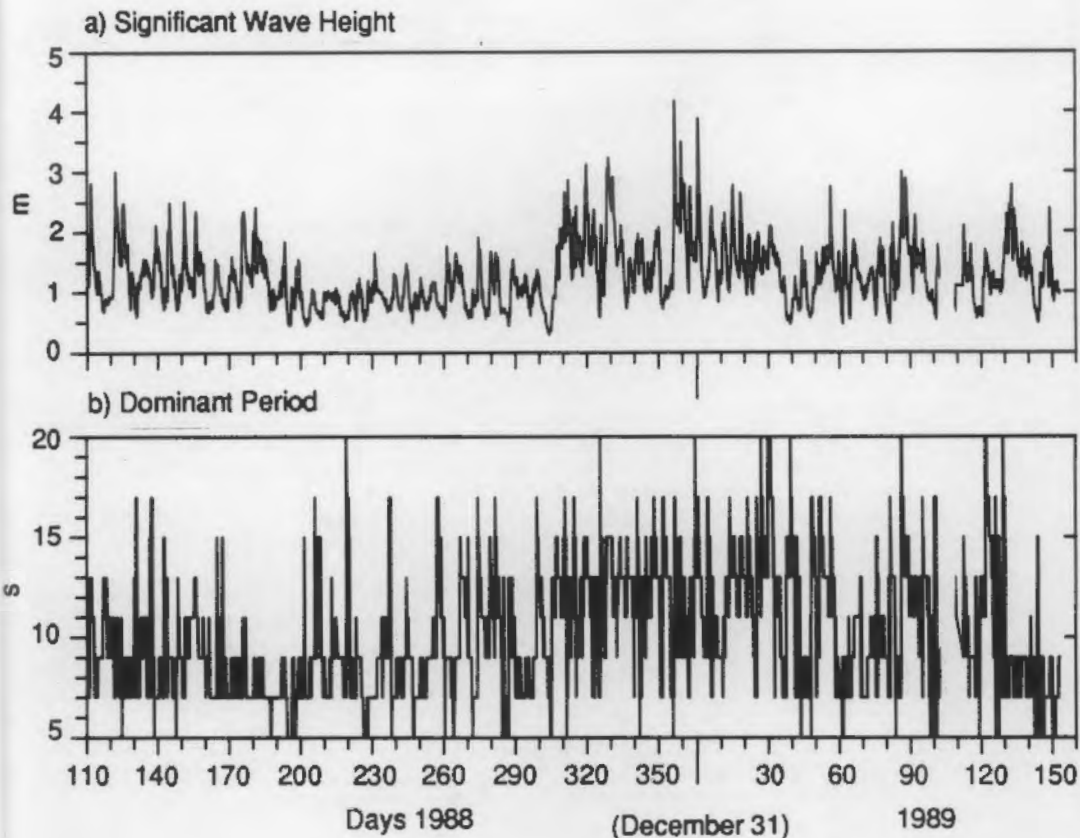
FIGURE 3.6.   Time Series of Significant Wave Height H_S and Wave
Period T at Montara

The spring transition began around March 31, 1989 (day 90). After this
date, temperatures recorded by the mid-depth and bottom instruments began to
fall, and strong, persistent southward currents were measured at Site B1B.
Upwelling, indicated by falling surface water temperatures, was established
by May 2 (day 122).

3.1.2 Statistical Summaries of Current Meter Data

Mean Monthly Flows

Monthly means were calculated for current velocities in the rotated
coordinate system. The results for the alongshore component are summarized
in Figure 3.7, and results for both components are tabulated in Volume 2,
Appendix B. Because most of the variation in the currents occurs on the

3.7

a) Site B1B

b) Site 1M
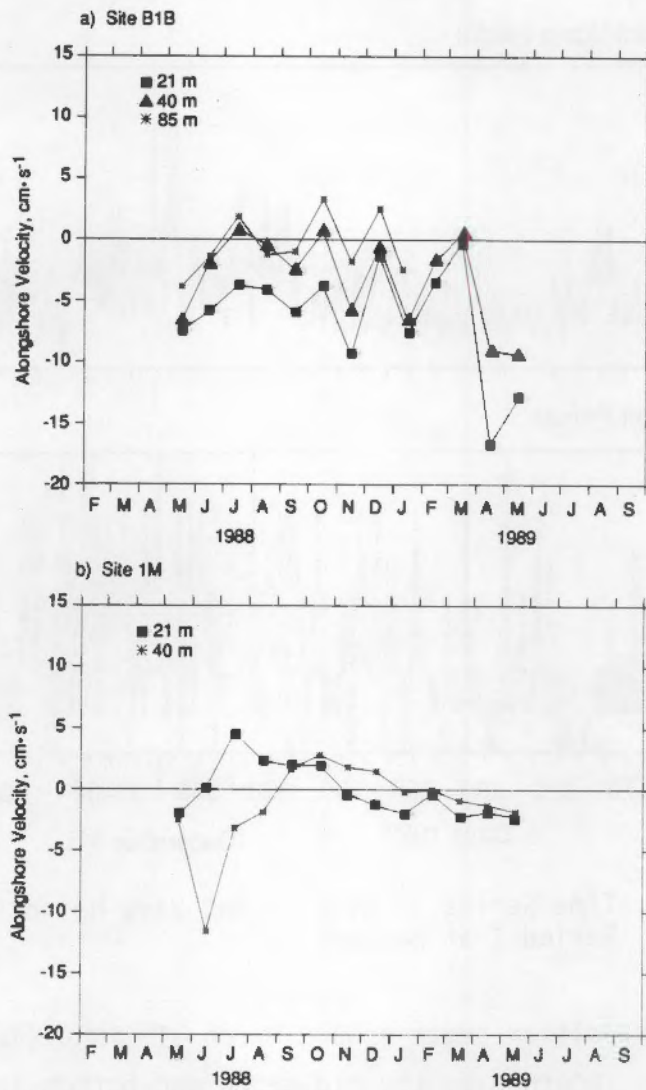
FIGURE 3.7. Monthly Mean Alongshore Current Velocities for Sites B1B and 1M

alongshore axis, estimates of the mean cross-shelf components are very sensitive to the coordinate system selected and will not be emphasized in the following discussion.

The monthly mean alongshore velocity at Site B1B was southward at 21 m for the entire measurement period, except for March 1989 when a very weak northward flow occurred. The velocity at 85 m was also weakly southward for much of the period. During July, October, and December 1989, however, the bottom velocity was northward. There was a very consistent velocity difference of 4 to 8 cm·s^{-1} between the 21-m measurement and the 85-m measurement,

3.8

with the strongest southward flow at 21 m. At Site 1M, the average along-
shore flow at 21 m was northward from June through November 1988 and at 40 m
was northward from September through December. The vertical velocity differ-
ence was greater than 5 to 10 $cm \cdot s^{-1}$ from June through August 1988, with the
strongest northward flow at 21 m. The velocity difference decreased to a few
$cm \cdot s^{-1}$ in September and October and reversed sign in December 1988. There
was northward flow at both depths from September through November 1988 and
southward flow at both depths from January through May 1989.

The observed alongshore velocities at Sites B1B and 1M are not con-
sistent with existing hypotheses for the seasonal circulation on the
California coast; this will be further discussed in Section 4.1.

Mean Current Velocities for the Study Period and By Season

Average current velocities measured by each instrument for the entire
study period are listed in Table 3.1. At Site B1B, mean flow was southward
at all depths, and velocities decreased with depth. Mean flows at 21 m and
46 m had slight onshore components, while at 85 m, mean flow was slightly

TABLE 3.1. Mean (and Standard Deviation) of Alongshore and Cross-Shelf
Components of Current Velocity, Mean Current Speed and
Direction, and Mean (and Standard Deviation) of Temperature
From All Instruments at Sites B1B and 1M for the Entire Study
Period

Depth	Alongshore[a] $v,$ $cm \cdot s^{-1}$	Cross-Shelf[b] $u,$ $cm \cdot s^{-1}$	Speed, $cm \cdot s^{-1}$	Direction, ^{o}T	Temperature, ^{o}C	Days
B1B, 21 m	-6.07 (10.72)	1.08 (9.22)	6.17	138	11.06 (1.06)	384
B1B, 46 m	-2.80 (10.14)	1.33 (7.49)	3.10	123	10.02 (0.88)	384
B1B, 85 m	-0.47 (7.67)	-0.71 (5.91)	0.85	205	9.24 (0.63)	262
1M, 21 m	0.64 (10.28)	1.12 (8.13)	1.29	28	10.41 (1.01)	364
1M, 40 m	-1.05 (7.09)	0.41 (6.16)	1.13	127	9.91 (0.83)	360

(a) Positive toward 328°T.
(b) Positive toward 58°T.

offshore. Mean current speed near the bottom (85 m) at Site B1B was 0.85 cm·s^{-1} toward 205°T. At Site 1M, flow near the bottom was southward and onshore, but at 21 m, flow was northward and onshore.

Seasonal averages for the alongshore component of current velocities at all instruments are summarized in Table 3.2. The seasons are spring/summer (May 15 to September 30) and fall/winter (November 1 to March 14). Data for CCCCS Mooring K and SuperCODE Mooring M3 are included on Table 3.2 for comparison and will be discussed in Section 4.0. The mean alongshore component is southward for all three depths at Site B1B in both seasons. At Site 1M, the mean flow near the bottom (40 m) is southward in spring/summer and weakly northward in fall/winter. Mean flow at 21 m at Site 1M, however, is the opposite: mean flow is northward in spring/summer and weakly southward in fall/winter. At both sites, the variation in current velocity decreased with depth.

TABLE 3.2. Seasonal[a] Means and Standard Deviations of Alongshore Velocity (cm·s^{-1}) at Sites B1B and 1M and Moorings K and H3

			Spring/Summer			Fall/Winter		
Station	Depth, m	Year	Mean	Standard Deviation	Days	Mean	Standard Deviation	Days
B1B, 21 m	21	88	-4.76	9.65	130	-4.34	10.31	123
B1B, 46 m	46	88	-1.21	9.53	130	-2.17	9.74	123
B1B, 85 m	85	88	-0.71	7.23	130	-0.61	7.75	80
1M, 21 m	21	88	2.70	10.43	130	-0.38	10.09	120
1M, 40 m	40	88	-3.10	7.52	127	0.49	6.81	119
M3S1[b]	35	81	0.74	6.54	119	4.47	7.52	117
M3S2	65	81	1.32	3.67	119	3.09	4.67	117
M3S1	35	82	-2.20	6.07	109			
M3S2	65	82	0.92	3.46	109			
K[c]	63	84	3.02	7.91	117	1.61	8.87	95

(a) Spring/Summer is May 15 to September 30.
    Fall/Winter is November 1 to March 14.
(b) SuperCODE Mooring H3 (Denbo and Allen 1987).
(c) CCCCS Mooring K (Chelton 1984).

Joint Probability Distributions: Current Speed and Direction

Joint probability distributions of current speed and direction provide a useful summary of current meter data. They indicate joint probability of occurrence for a specific combination of current speed and direction. The information is presented in several graphical formats as Figures 3.8 and 3.9 and is tabulated in Volume 2, Appendix B. Scatter plots of the 40-h low-pass filtered current velocities at Sites B1B and 1M are presented on the left-hand side of Figures 3.8 and 3.9. The scatter plots are created by plotting a single point for each velocity observation at 6-h intervals. Each point marks the tip of a current vector pointed in the direction toward which the current flowed over the 6-h period. The length of the vector is proportional to the current speed and can be determined using the bar scale shown beneath the plots. The shape and density of the cloud of points provides a visual indication of the frequency of flows in any given direction. The joint probability distribution visually suggested by the cloud of points can be quantified in several ways, two of which also appear in Figures 3.8 and 3.9 and are discussed below.

The first method of quantifying speed and direction data shown in the scatter plots is principal component analysis. The crosses to the right of the scatter plots indicate the principal axes of variation in the current velocities. The longer of the two axes indicates the direction in which most of the variation in the current velocities occurs; the length of the axis is proportional to the variance of currents in that direction. The remaining variation in the velocity records is contained in the second axis, which is oriented at a 90° angle to the primary axis. In a perfectly reversing current system, such as a narrow tidal channel, all of the variation would occur along the primary axis, which would be oriented along-channel. On the other hand, currents that are evenly distributed in every direction, such as rotary tidal currents, would have axes of equal length.

The contour plots shown on the right side of Figures 3.8 and 3.9 represent a second method for quantifying speed and direction data. Contours represent the probability of finding the tip of a current vector in a region

3.11
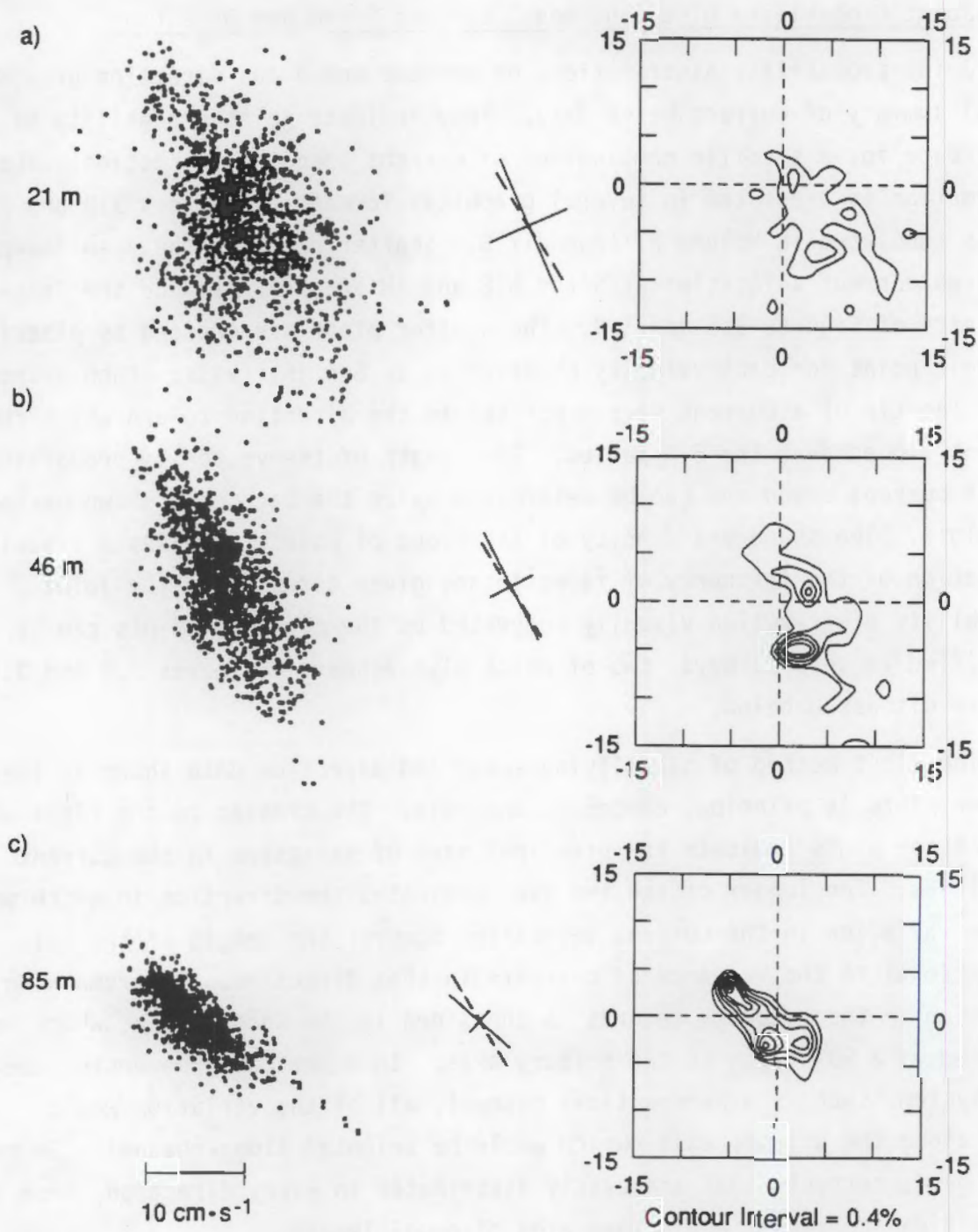
FIGURE 3.8. Scatter Plots, Principal Component Axes, and Joint Probability Contour Plots for 40-h Low-Pass Filtered Currents at Depths of 21 m, 46 m, and 85 m, Site B1B. Dashed line indicates axis of alongshore flow.
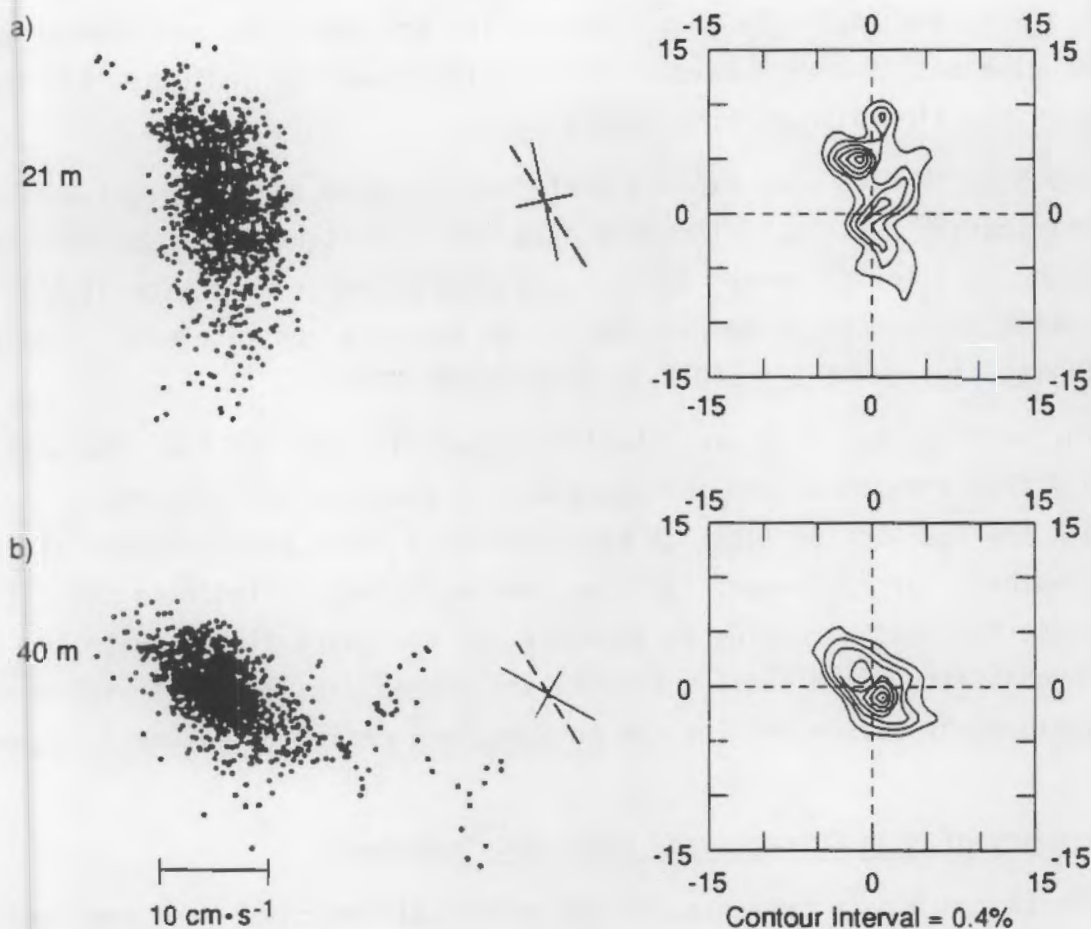
FIGURE 3.9. Scatter Plots, Principal Component Axes, and Joint Probability Contour Plots for 40-h Low-Pass Filtered Currents at Depths of 21 m and 40 m, Site 1M. Dashed line indicates axis of along-shore flow.

of the plot. Areas representing frequently occurring current vectors appear as bumps of high probability on the contour plots. In other words, the contours quantify the density of points on the scatter plots.

The scatter plots and contour plots for Site B1B (Figure 3.8) are elongate in the alongshore direction, indicating that flows are nearly parallel with the alongshore axis, which points, by convention in this report, toward 328°T. The ellipse defined by the principal component axes becomes more narrow and elongate with depth, indicating that currents are increasingly oriented alongshore near the bottom. For the 85-m data, the contour plot suggests that the most probable flow directions are toward

3.13

305°T, 195°T, and 140°T (in that order). The scatter plots and contour plots for the 21-m and 46-m data have a less regular shape and indicate that the most probable flow direction is toward 160°T.

The Site 1M data also exhibit preferred alongshore flow directions, but the distribution pattern of the 40-m data has a substantial cross-shelf component and is oriented toward 315°T. The most probable direction at this near-bottom instrument is toward 145°T. An irregular pattern with a maximum probability of flow toward 340°T is observed at 21 m.

The joint probability distributions generally indicate that the most probable flow directions are in approximately alongshore directions. Although the near-bottom flows at each site have about equal probability of being southward or northward, the shallower measurements indicate definite preference for southward flow at Site B1B and northward flow at Site 1M. The joint probability distributions for the unfiltered data from all instruments are tabulated by season and for the entire study period in Volume 2, Appendix B.

Summary of Mean Currents and Principal Components

The 13-month mean currents and the principal component axes are summarized in Figure 3.10. This figure clearly shows the alignment of principal axes in the alongshore direction and the southward mean flow measured at all locations except the upper (21-m) instrument at Site 1M.

3.1.3 Frequency-Domain Statistics

Several statistical techniques were used to analyze the frequency content of the time series data. Time series can be represented in the frequency domain as combinations of oscillations with specified amplitudes and frequencies. The advantage of the frequency-domain approach is that some of the forcing mechanisms that generate currents, such as tides and winds, are associated with specific frequency bands, and the presence of oscillations in these bands is evidence for the influence of these forcing mechanisms. Frequency domain statistics used in this study include autospectra for individual time series, cross-spectra and coherence for pairs of time series,
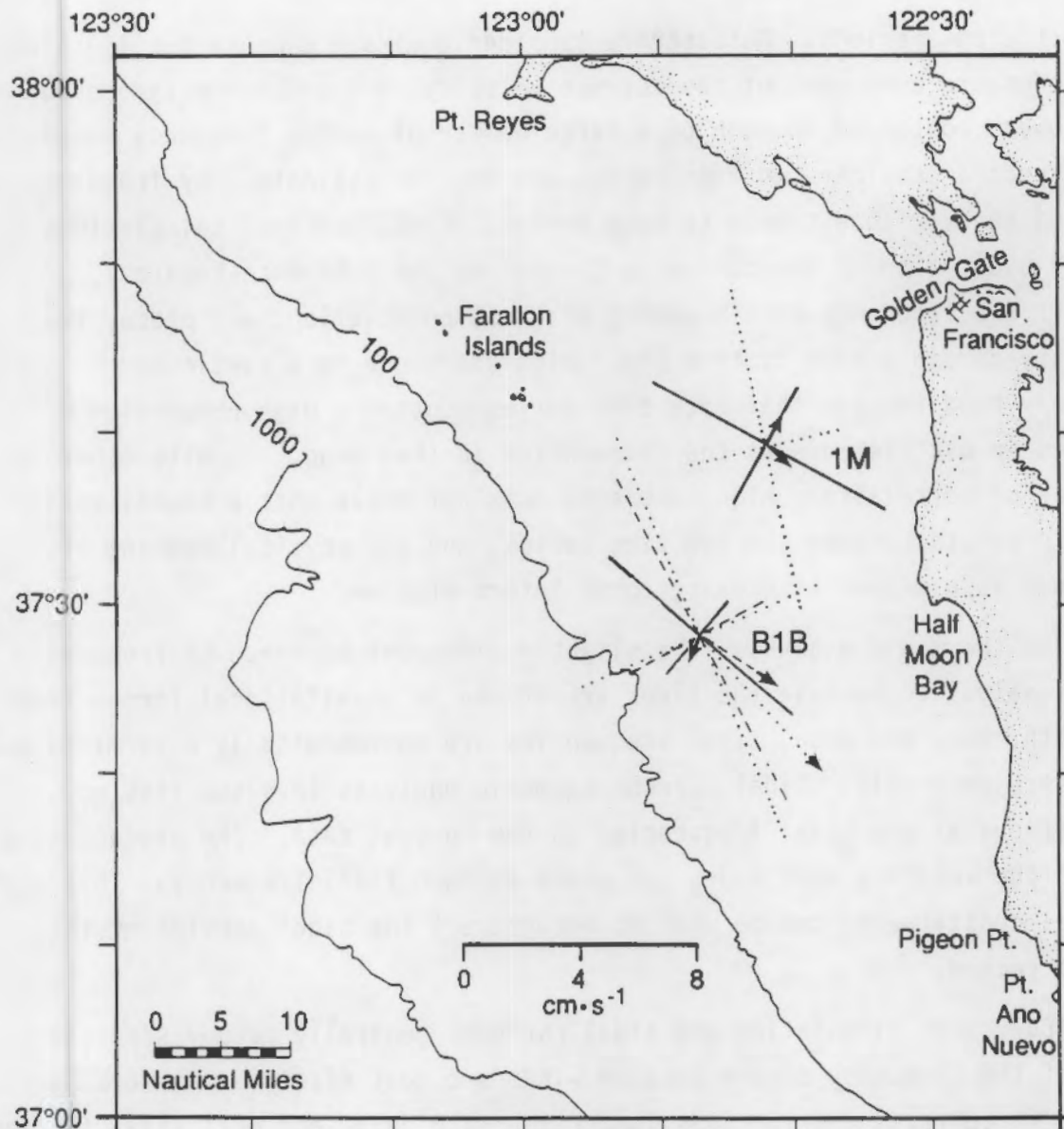
FIGURE 3.10. Mean Current (Arrows) and Principal Axes of Variation Calcu-
lated for Entire 13-Month Data Set at Sites B1B and 1M.
Data from instruments at 21-m depths are shown with dotted
lines, near-bottom data are shown with solid lines, and
46-m data at Site B1B are shown with dashed lines.

and tidal harmonic analysis for current velocity time series. A description
of the techniques used and complete presentation of the results are provided
in Volume 2, Appendix B.

Autospectra provide an indication of the relative importance (in terms
of contribution toward the total variance of the time series) of oscillations

with different periods. Autospectra consider a single time series (such as the alongshore component of the current velocity) and provide estimates of the "power" contained in each of a large number of narrow frequency bands. Cross-spectra consider two time series and provide estimates, by frequency band, of the variance common to both series. Cross-spectral calculations include estimation of the coherence (formally, the coherence-squared), which is the frequency-domain analog of cross-correlation, and phase, the frequency-domain analog of time lag. High coherence in a particular frequency band implies that both time series contain a high proportion of variance in oscillations at the frequencies in that band. As with other measures of correlation, high coherence does not prove that a causal relationship exists between the two time series, and the physical meaning of coherence is a matter of oceanographic interpretation.

Tidal harmonic analysis is a slightly different approach to frequency-domain analysis. Because the tides are driven by gravitational forces from the earth, sun, and moon, tidal frequencies are astronomically determined and known very precisely. Tidal current harmonic analysis involves fitting oscillations at the tidal frequencies to the current data. The product is a list of the velocity amplitudes and phase at each tidal frequency. This list of tidal constituents can be used to reconstruct the tidal portion of the current record.

Wind-driven circulation and tidal currents generally occupy separate parts of the frequency domain because winds are most effective at forcing changes in currents over periods longer than 1.5 days, and most tidal forcing occurs at periods of about 1 day (diurnal) and about 1/2 day (semidiurnal). The autospectra for the five current meters have very similar characteristics (Figure 3.11). The very strong peaks that appear in the diurnal and semi-diurnal bands have a nearly equal amount of variance in the alongshore (v) and cross-shelf (u) velocity components, except for near the bottom at both sites. This is characteristic of rotary tidal currents. In the wind-forced band, variance increases as period increases, and most of the variance in the wind-forced band occurs in the alongshore component at periods of 4 days and longer. This is consistent with the tendency for low-frequency shelf currents to flow along bathymetric contours. The following sections will

3.16
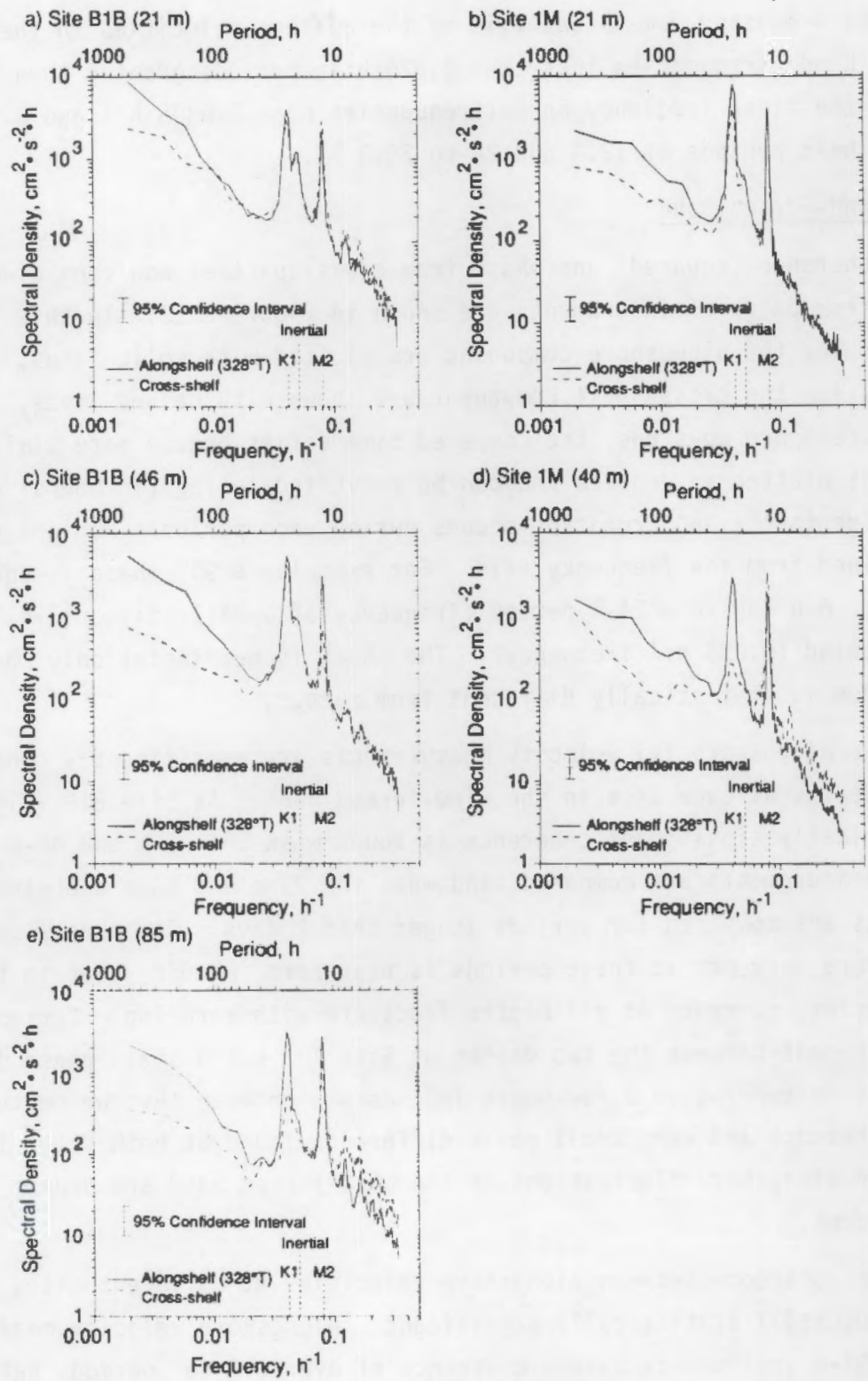
FIGURE 3.11.   Autospectra for Alongshore (——) and Cross-Shelf (— — —)
Components of Current Velocity at Site B1B and Site 1M

describe frequency-domain analysis of the current velocities in the wind-forced band (frequencies less than 0.025 h^{-1}; periods greater than 1.6 days) and in the tidal frequency band (frequencies near 0.0805 h^{-1} and 0.0418 to 0.0387 h^{-1}; periods of 12.4 and 24 to 25.8 h).

Wind-Forced Band

Coherence (squared) and phase from cross-spectral analyses of measurements from pairs of instruments are shown in Figure 3.12. In this figure, results for the alongshore component are plotted with solid lines, and results for the cross-shelf component are shown with dashed lines. As coherence approaches one, the compared time series become more similar. Phase is plotted in degrees and can be converted to lag (in hours) using the knowledge that a 360° rotation occurs during each period. Periods can be determined from the frequency axis. For example, a 90° phase is equal to 1/4 period: 6-h lag in a 24-h period (frequency of 0.0417 h^{-1}) or 3-h lag in a 12-h period (0.083 h^{-1} frequency). The phase is meaningful only when the coherence is statistically different from zero.

The alongshore (v) velocity measurements are significantly coherent among depths at each site in the wind-forced band. At Site B1B (Figure 3.12) statistically significant coherence is found when the 21-m and 46-m alongshore measurements are compared, and when the 21-m and 85-m alongshore measurements are compared for periods longer than 2 days. The phases between alongshore currents at these periods is near zero, meaning that in these low frequencies, currents at all depths fluctuate with zero lag. Currents are also coherent between the two depths at Site 1M, but a small phase difference, corresponding to a few hours lag, occurs between the two depths. The high coherence and very small phase difference found at both sites indicates that the alongshore fluctuations in the wind-forced band are depth independent.

The coherence between alongshore velocities at different sites is much lower but still statistically significant. Alongshore velocity measurements at the 21-m instruments have a coherence of over 0.2 for periods between 2 and 10 days. The phase difference at the 4-day period is equivalent to a 0.5-day lag. Cross-spectral calculations for other combinations of the

3.18
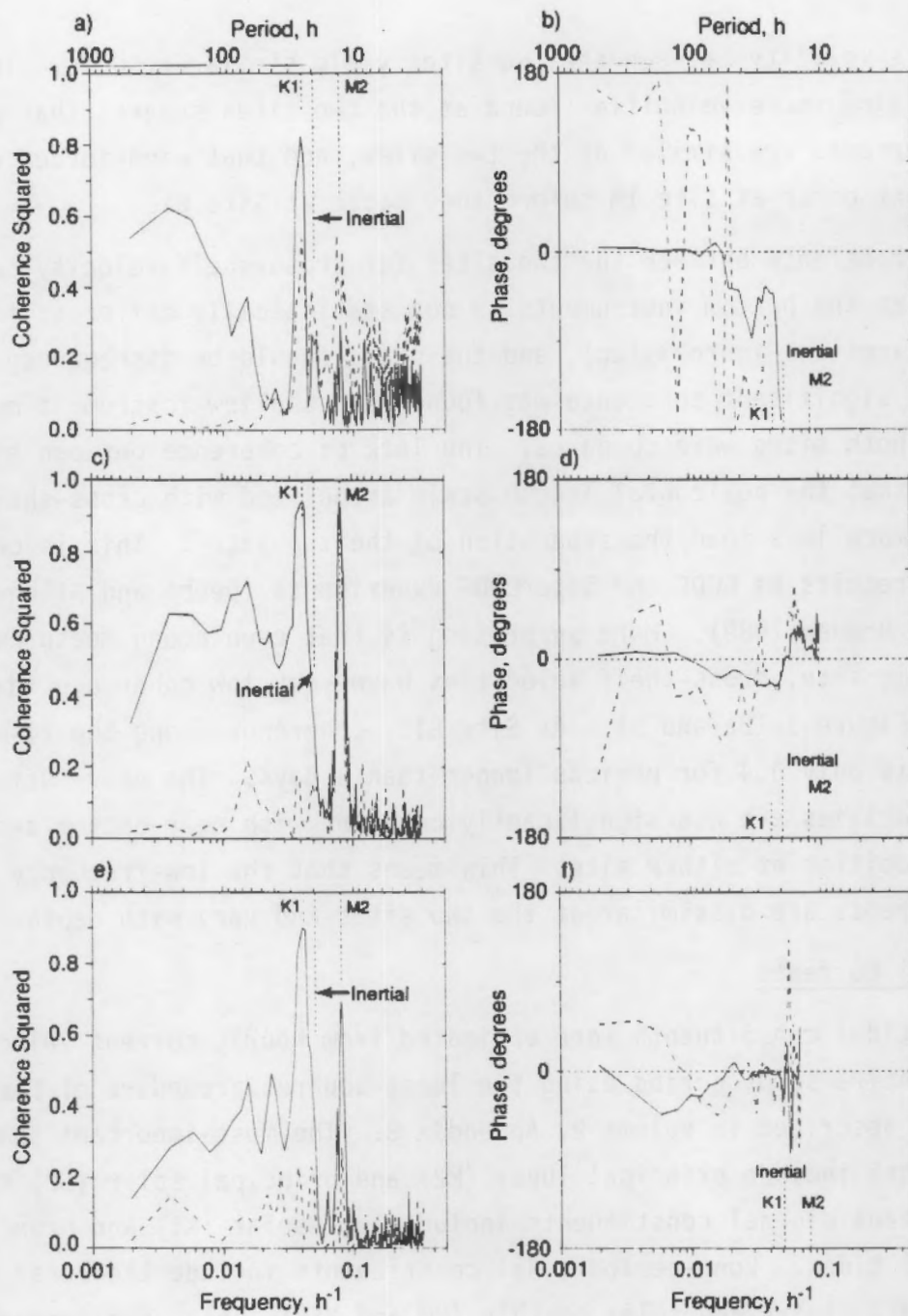
FIGURE 3.12. Coherence (squared) and Phase from Cross-Spectral Analysis of
Alongshore (———) and Cross-Shelf (— — —) Components of
Current Velocity Among Pairs of Instruments: (A and B)
Site B1B (21 m) with Site B1B (85 m); (C and D) Site 1M
(21 m) with Site 1M (40 m); (E and F) Site B1B (85 m) with
Site 1M (40 m)

3.19

alongshore velocity between the two sites yield similar results. The coherent alongshore velocities found at the two sites suggest that wind-forced currents are similar at the two sites, and that wind-forced changes in the current occur at Site 1M before they occur at Site B1B.

The coherence between the two sites for cross-shelf velocity components measured at the bottom instruments is not statistically different from zero (dashed lines on Figure 3.12c), and the phase should be disregarded. Similarly, no significant coherence was found when shallow-instrument measurements at both sites were compared. The lack of coherence between sites suggests that the horizontal length scale associated with cross-shelf currents is much less than the separation of the two sites. This is consistent with the results of CODE and SuperCODE experiments (Denbo and Allen 1987; Davis and Bogden 1989). More surprising is that even among measurements made at the same site, cross-shelf velocities have very low coherence (dashed lines on Figure 3.12a and b). At Site B1B, coherence among the 21-m and 46-m currents is only 0.4 for periods longer than 8 days. The near-surface cross-shelf velocities are not significantly coherent with near-bottom cross-shelf velocities at either site. This means that the low-frequency cross-shelf currents are dissimilar at the two sites and vary with depth.

Tidal Currents

The tidal constituents were estimated from hourly current velocities for the entire study period using the least-squares procedure of Foreman (1978) as described in Volume 2, Appendix B. The most important semidiurnal constituents include principal lunar (M2) and principal solar (S2) tides, and the important diurnal constituents include luni-solar (K1) and principal lunar (O1) tides. Long-period tidal constituents include the lunar fortnightly (MF), lunar and solar monthly (MM and MSM), solar semi-annual (SSA), and solar annual (SA) tidal constituents. The analysis also calculates the mean current (Z0), which differs slightly from the means presented in Table 3.1 because the tidal calculations are based on hourly data and the tidal analysis removes large annual and semiannual components from records that are not exactly a year in length. Tables 3.3 through 3.7 summarize the largest diurnal and semidiurnal constituents found at each instrument.

3.20

TABLE 3.3. Primary Tidal Components for Site B1B (21 m) April 27, 1988, 1600 through June 2, 1989, 2400 (Greenwich Phases are for Time Zone GMT)

| Name | Period, h | Amplitude | | Greenwich Phase, ° | | | |
		Major, $cm \cdot s^{-1}$	Minor, $cm \cdot s^{-1}$	Inc	G	G+	G-
Principal Lunar Diurnal (O1)	25.82	2.99	1.54	11.5	89.1	77.6	100.7
Luni-Solar Diurnal (K1)	23.93	5.32	1.96	5.3	127.3	122.0	132.6
Principal Lunar Semidiurnal (M2)	12.42	3.63	-2.86	102.6	23.8	281.2	126.3

TABLE 3.4. Primary Tidal Components for Site B1B (46 m) April 27, 1988, 1600 through June 2, 1989, 2400 (Greenwich Phases are for Time Zone GMT)

| Name | Period, h | Amplitude | | Greenwich Phase, ° | | | |
		Major, $cm \cdot s^{-1}$	Minor, $cm \cdot s^{-1}$	Inc	G	G+	G-
Principal Lunar Diurnal (O1)	25.82	3.24	1.52	13.9	82.6	68.8	96.5
Luni-Solar Diurnal (K1)	23.93	6.05	3.09	7.5	128.3	120.9	135.8
Principal Lunar Semidiurnal (M2)	12.42	4.45	-1.32	163.4	331.6	168.2	134.9

TABLE 3.5. Primary Tidal Components for Site B1B (85 m) April 27, 1988, 1600 through January 20, 1989, 2400 (Greenwich Phases are for Time Zone GMT)

| Name | Period, h | Amplitude | | Greenwich Phase, ° | | | |
		Major, $cm \cdot s^{-1}$	Minor, $cm \cdot s^{-1}$	Inc	G	G+	G-
Principal Lunar Diurnal (O1)	25.82	2.23	0.88	156.6	289.6	132.9	86.2
Luni-Solar Diurnal (K1)	23.93	3.75	1.12	144.1	337.7	193.6	121.8
Principal Lunar Semidiurnal (M2)	12.42	4.84	-0.26	173.2	347.8	174.6	161.0

TABLE 3.6. Primary Tidal Components for Site 1M (21 m) May 8, 1988, 1300 through May 27, 1989, 1700 (Greenwich Phases are for Time Zone MT)

| Name | Period, h | Amplitude | | Greenwich Phase, ° | | | |
		Major, $cm \cdot s^{-1}$	Minor, $cm \cdot s^{-1}$	Inc	G	G+	G-
Principal Lunar Diurnal (O1)	25.82	4.53	2.15	4.1	94.8	90.7	98.8
Luni-Solar Diurnal (K1)	23.93	7.45	2.50	0.5	135.4	134.9	135.9
Principal Lunar Semidiurnal (M2)	12.42	8.27	-0.58	14.2	135.3	121.1	149.5

TABLE 3.7. Primary Tidal Components for Site 1M (40 m) May 8, 1988, 1300 through June 2, 1989, 2400 (Greenwich Phases are for Time Zone GMT)

| Name | Period, h | Amplitude | | Greenwich Phase, ° | | | |
		Major, cm·s^{-1}	Minor, cm·s^{-1}	Inc	G	G+	G-
Principal Lunar Diurnal (O1)	25.82	2.45	0.37	162.4	287.0	124.6	89.3
Luni-Solar Diurnal (K1)	23.93	4.04	-0.01	150.3	325.7	175.4	116.0
Principal Lunar Semidiurnal (M2)	12.42	6.19	-1.52	22.1	112.5	90.4	134.6

Complete tabulation of the results is included in Volume 2, Appendix B. Disregarding the mean, the M2 and K1 are the two largest tidal constituents observed at the two sites, and discussion will be restricted to these two constituents.

Principal Lunar Semidiurnal (M2) Constituent

Tidal ellipses for the M2 tides at each instrument are shown in the top panels of Figure 3.13. The ellipses describe the path that the tip of a velocity vector will trace over the 12.42-h period associated with the M2 tide. The ellipses are plotted relative to geographical north, not the rotated coordinate system used in most of this report. The point on the ellipse that corresponds to the velocity vector position at 0000 h Greenwich Mean Time (GMT) is shown as a radial line that intersects the ellipse. The direction of rotation for the velocity vector is indicated by the orientation of the barb at the end of the line.

At Site B1B, the velocity vectors rotate clockwise, making one revolution every 12.42 h. The tidal ellipses become more elongate with depths: the ellipse at 21 m is nearly circular and oriented toward 348°T, but at the bottom (85 m) the ellipse is elongate and rotated westward toward 277°T. The tidal ellipse at 85 m forms an angle of about 50° with the regional trend of the depth contours. At any instant, tidal currents near the surface lead those at depth, and the orientations of the velocity vectors shift counterclockwise with depth. At Site 1M the velocity vectors also rotate clockwise over the course of the tidal cycle, and currents at the surface lead those at depth. However, both M2 tidal ellipses at Site 1M are very elongate along an axis from west-southwest to east-northeast, and the bottom ellipse is approximately perpendicular to the regional depth contours.
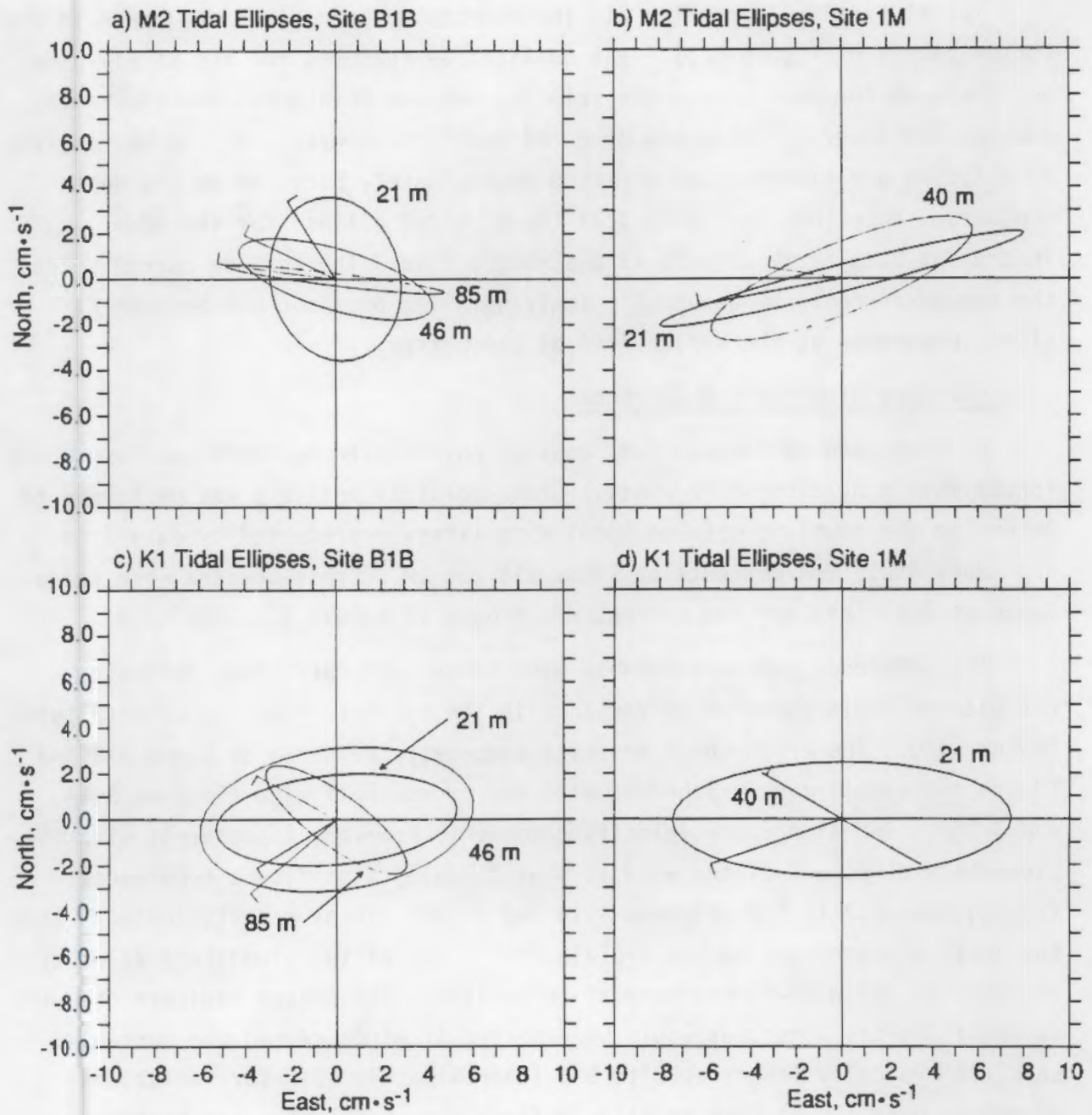
FIGURE 3.13. Computed Tidal Current Ellipses for Principal Lunar Semidiurnal (M2) and Luni-solar Diurnal (K1) Tidal Constituents at Sites B1B and 1M. The ellipses trace the tip of the tidal current velocity vectors in an geographic coordinate system relative to true north. The radial lines mark the orientation of the vector at 0000 h Greenwich mean time (GMT), and the barb (———⌐) on the radial line points in the direction of rotation.

3.23

Luni-Solar Diurnal (K1) Constituent

The K1 tidal ellipses for all instruments at both sites are shown in the bottom panels of Figure 3.13. The qualitative features for the K1 ellipses are the same for each site. The velocity vectors rotate counter-clockwise, and the shallower ellipses are oriented nearly east-west. At the bottom, the K1 ellipses are elongate and oriented approximately parallel to the depth contours. Note that in Figure 3.13 the K1 tidal ellipse for the 40-m instrument at Site 1M appears as a straight line. The shallow currents lead the deeper currents by about 90°, implying a lag of about 6 h between K1 tidal components at the surface and at the bottom.

Coupling of Winds and Currents

As discussed in Section 1.0, coastal currents in northern California are forced mostly by alongshore winds. Cross-spectral analysis was performed to determine the coupling between local wind stress represented by data from NDBC Buoy 46012 and currents at Sites B1B and 1M. Cross-spectra were calculated as described for the current meter data in Volume 2, Appendix B.

The coherence computed between wind stress and currents provides an estimate of the proportion of variance in the currents that can be attributed to the wind. The cross-shelf velocity components measured at Sites B1B and 1M are not significantly coherent with the cross-shelf wind (Figures 3.14 and 3.15). The alongshore velocity component, however, is coherent with the alongshore component of the wind at statistically significant coherences ranging from 0.2 to 0.6 (Figures 3.14 and 3.15). These results indicate that the local alongshore wind can explain 20% to 60% of the alongshore velocity variance in the wind-forced band at both sites. The phases indicate that the currents lag the winds, as would be expected if winds caused the currents. Lags are typically longer at Site B1B (approximately 12 h for variations occurring over 100 h) than at Site 1M (less than 6-h lag). The highest coherences were found between the wind and the near-bottom (85-m) currents at Site B1B, but these coherences were based on the shortest period of record.

3.24
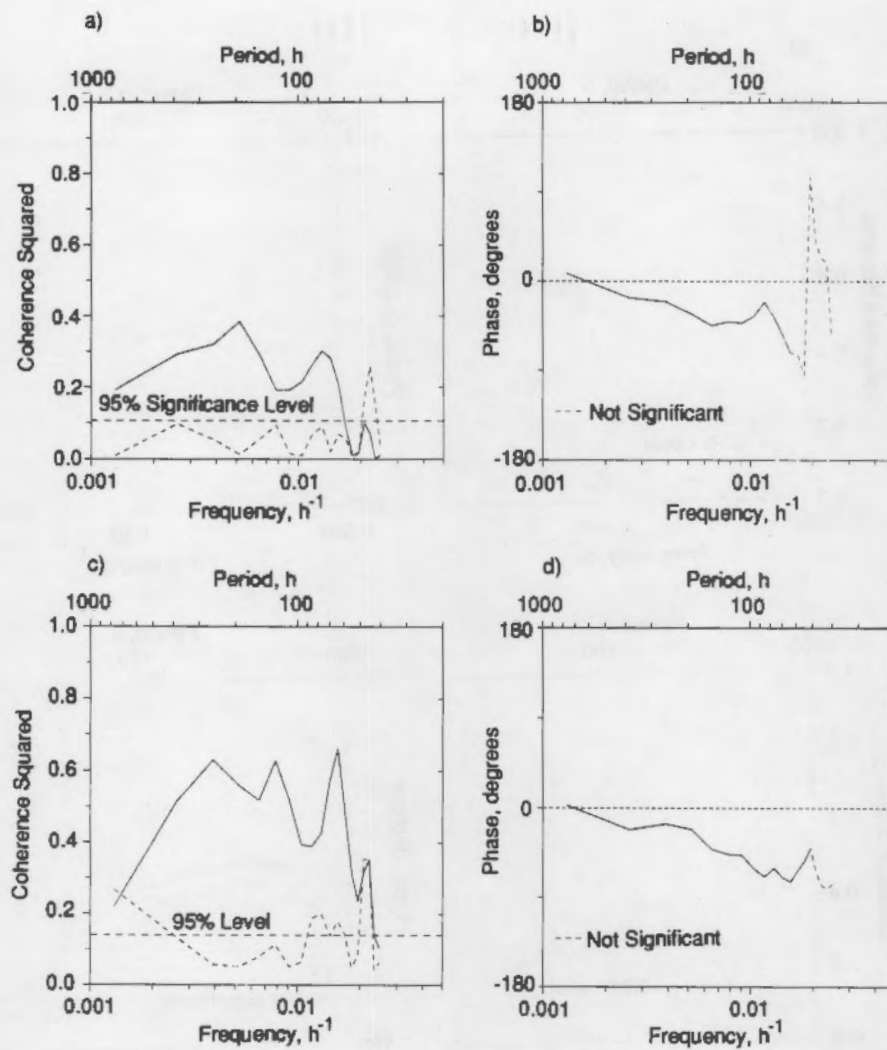
FIGURE 3.14. Coherence and Phase from Cross-Spectral Analysis of Alongshore
(————) and Cross-Shelf (— — —) Components of Current
Velocity at Site B1B with Wind Stress Calculated at NDBC
Buoy 46012: (A and B) Site B1B (21 m) with Wind at
Buoy 46012; (C and D) Site B1B (85 m) with Wind at
Buoy 46012

Summary of Frequency-Domain Statistics

Overall, 70% to 80% of the variance in currents measured at Sites B1B
and 1M is related to the combined effects of tides and wind stress.
Table 3.8 summarizes the distribution of variance in the alongshore currents.
The variance is tabulated for the low frequency band (<0.6 d^{-1}) and for the
tidal frequency bands (diurnal, which includes the tidal and inertial bands,
and semidiurnal tidal frequencies). Nearly half of all of the variance at

3.25
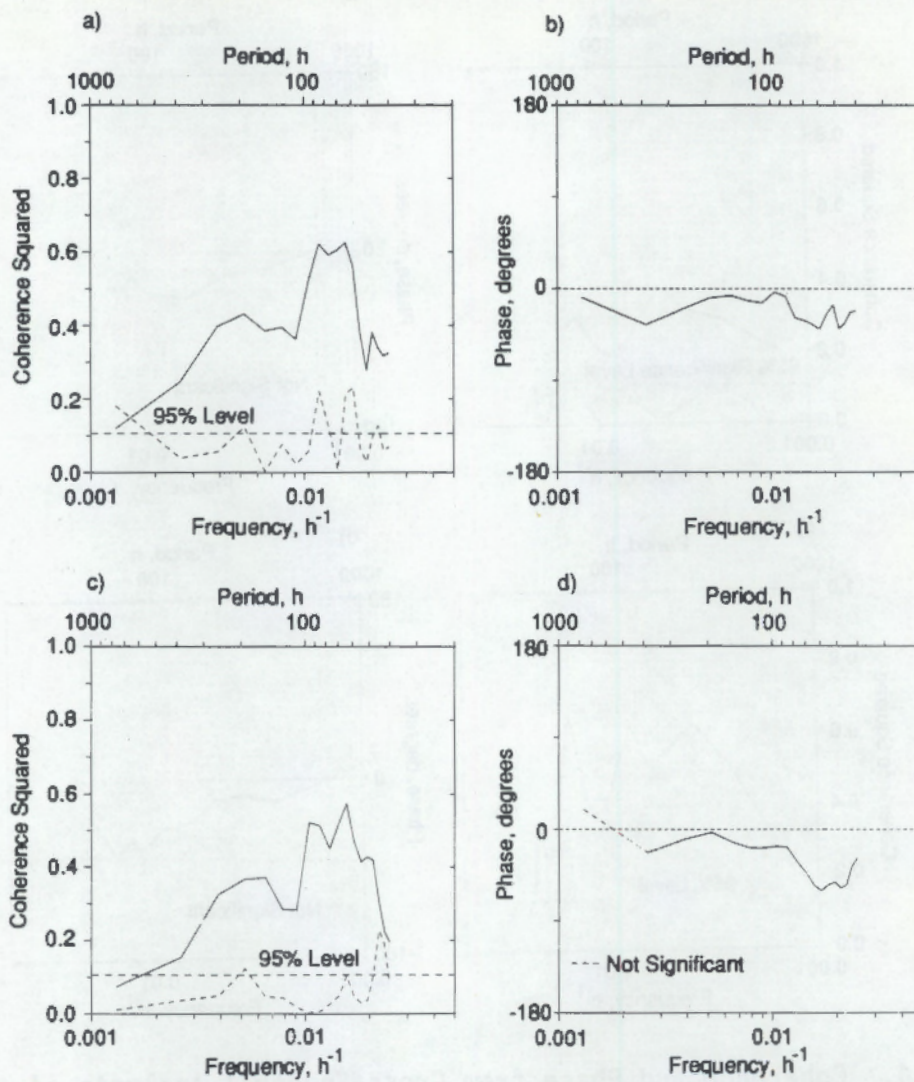
FIGURE 3.15. Coherence and Phase from Cross-Spectral Analysis of Alongshore
(———) and Cross-Shelf (— — —) Components of Current
Velocity at Site 1M with Wind Stress Calculated at NDBC
Buoy 46012: (A and B) Site 1M (21 m) with Wind at Buoy 46012;
(C and D) Site 1M (40 m) with Wind at Buoy 46012

TABLE 3.8. Average Percentage of Alongshore Variance by Frequency Band

| | Frequency Band | | |
| | | Tidal | |
Station	Low (<0.6 d^{-1})	(0.91$<$f$<$1.3 and 1.9$<$f$<$2.1 d^{-1})	Total
B1B, 21 m	42	42	84
B1B, 46 m	31	55	86
B1B, 85 m	27	53	80
1M, 21 m	22	71	93
1M, 40 m	25	67	92

Site B1B is in the tidal frequency bands: tides account for 42% of the
variance at 21 m, 55% at 46 m, and 53% at 85 m. At Site 1M, tides account
for an even larger proportion of the measured variance: at 21 m, tides
account for 71% of the variance, and at 40 m, 67% of the variance. At both
sites, winds account for 40% to 50% of the variance over periods between 2
and 10 days. These results imply that, while local winds do affect low-
frequency currents, knowledge of local winds is not sufficient for making
accurate predictions of low-frequency currents.

3.2 SEDIMENT TRANSPORT CALCULATIONS

Sediment transport calculations were made using current velocity data
from the near-bottom current meters at Sites B1B and 1M. Wave data recorded
at the nearby Montara pressure-gage array and provided by the Coastal Data
Information Program were also used in the calculations. The calculations
employed a model developed by Grant and Madsen (1979) for determining the
combined bottom shear stress resulting from the interaction among waves and
currents at the sea bed. The model makes specific assumptions about the
nature of turbulent flow near the bed and predicts that the bottom shear
stress at the sea bed arises from a combination of currents and the oscil-
latory motion of waves. The model also includes a parameterization of the
turbulent diffusion processes responsible for vertical transport of momentum
and suspended sediment near the bottom. An alternative method for solving
the equations of the Grant and Madsen (1979) model was used. The solution
was presented by Larsen et al. (1981) and used successfully in predicting

3.27

suspended sediment concentrations in several continental shelf environments (Shi et al. 1985). A more complete description of the wave-current boundary layer model is contained in Volume 2, Appendix C of this report.

The wave-current boundary layer model was used with input data for waves, currents, and bottom sediment type to predict bottom shear stress, which is the tangential force responsible for the erosion and near-bottom transport of material. It also allowed estimates of the suspended-sediment profile and, therefore, could be used to make suspended-sediment transport calculations. Bedload sediment transport was not calculated because it represents only a small fraction of the total sediment transport at most west-coast continental shelf sites (Kachel and Smith 1986). The much greater fraction is suspended-sediment transport. Suspended-sediment transport was calculated on an hourly basis as the product of calculated suspended-sediment concentration profiles and velocity profiles. The velocity profiles were derived directly from the solution of the wave boundary layer model; the suspended-sediment profiles were calculated using the bottom shear stress from the model and by assuming a steady-state balance between upward diffusion and downward settling of sediment particles.

Input to the sediment transport calculations included hourly near-bottom current velocity data and estimates of the near-bottom wave-orbital velocity. Current measurements from the near-bottom instruments were filtered with the 3-h low-pass filter described in Volume 2, Appendix B and resampled at hour intervals. Wave-orbital velocities were estimated from surface-wave spectra by first using linear wave theory to calculate a near-bottom wave-orbital velocity amplitude spectrum from the surface wave spectrum, and then calculating a "significant" orbital-velocity amplitude from the variance of the spectrum. The period chosen for the significant wave-orbital velocity amplitude was that of the dominant amplitude in the orbital-velocity spectrum. This procedure (described in detail in Volume 2, Appendix C) preserved low-frequency motions associated with longer-period waves. The final inputs required were the characteristics of the bottom sediments. Four grain-size classes were used to approximate the sediment distribution measured in bottom grab samples from the sites, and characteristics for natural, noncohesive

3.28

sand and coarse silt were used. Selection of other parameters and coefficients were based on literature values and sensitivity analyses, and are discussed in Volume 2, Appendix C.

The sediment transport calculations yield time series of estimated bottom shear stress τ_{cw}, and bottom shear velocity $u*_{cw}=(\tau_{cw}/\rho)^{\frac{1}{2}}$. Bottom material available for transport will move whenever the bottom shear velocity exceeds the critical value $u*_{crit}$. The critical shear velocity $u*_{crit}$ is a property of the in situ bottom material. When $u*_{cw}$ exceeds $u*_{crit}$, a suspended sediment profile is calculated and the suspended-sediment flux for all sediment in the lower 10 m of the water column is determined using the concentration profile and the velocity profile. Thus the calculations also yield a time series of sediment concentration and a time series of sediment flux. In the model, the direction of the instantaneous sediment flux at each hour is always aligned with the instantaneous current direction.

3.2.1 Bottom Shear Velocity

Plots of calculated bottom shear velocity $u*_{cw}$ (Figures 3.16a and 3.16b) essentially summarize the forces controlling sediment resuspension. Occurrence of resuspension events can be identified as points in the time series when the calculated shear velocity is greater than the critical shear velocity. For example, the calculations for Site B1B suggest that sediment with a critical shear velocity of 2.0 cm·s^{-1} would have moved only during two events in December. There is a close correlation apparent between the calculated time series of $u*_{cw}$ values and time series of wave orbital velocities used as input for the calculations (Volume 2, Appendix C). A much smaller correlation is observed between $u*_{cw}$ and the time series of near-bottom current speed used as input (Volume 2, Appendix C). This suggests that waves were responsible for most of the bottom shear stress during the study period. Calculated $u*_{cw}$ varies seasonally and is generally lower during the summer months and higher in the winter.

The cumulative probability distributions of calculated sheer velocity $u*_{cw}$ for Sites B1B and 1M are shown in Figure 3.17. These curves can be used

3.29
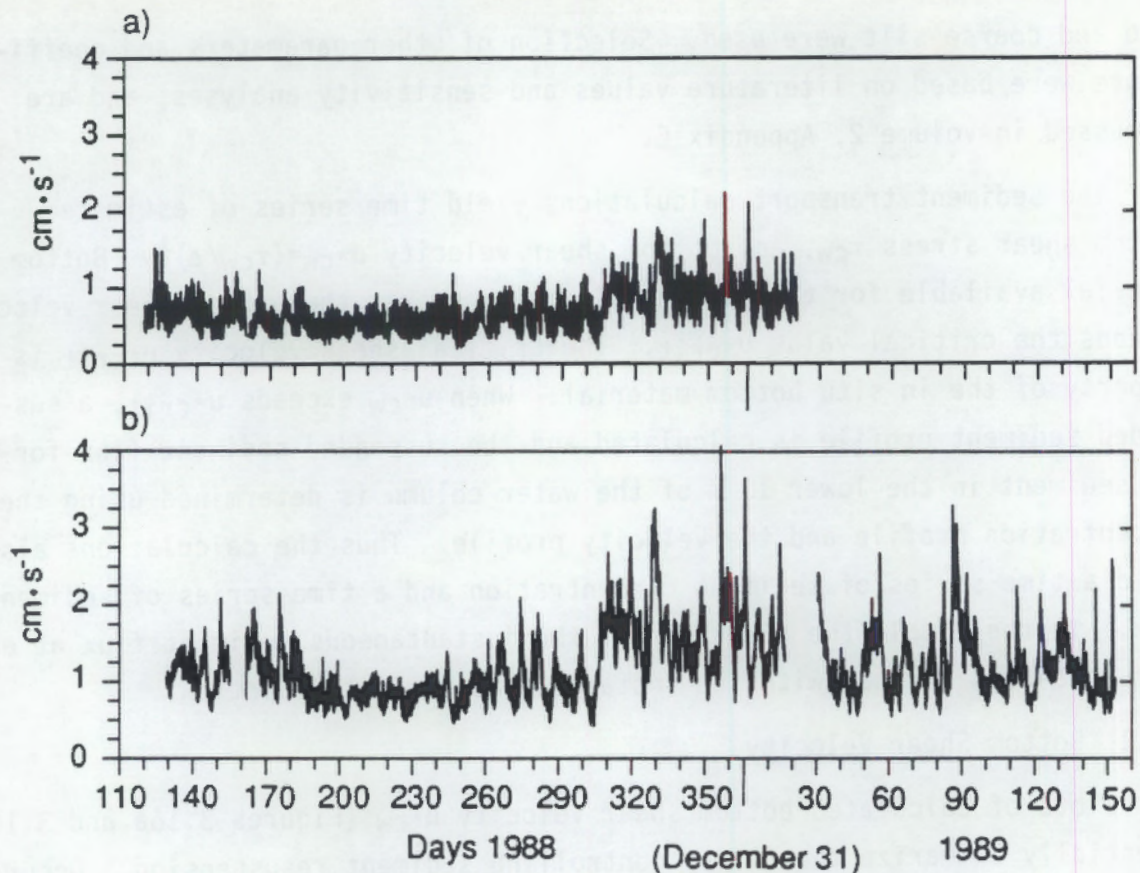
FIGURE 3.16. Time Series of Calculated Combined Shear Velocity $u*_{cw}$ at a) Site B1B and b) Site 1M

to estimate the probability of encountering bottom shear velocities of any specified value. Calculated $u*_{cw}$ values are substantially higher at Site 1M. Mean shear velocity at Site 1M was 1.2 cm·s^{-1}, and at Site B1B was 0.7 cm·s^{-1}. The higher shear velocities at Site 1M are related to the shallower depth, which allows shorter period wave-induced motions to reach the bottom and results in higher wave-orbital velocity amplitudes for waves of all periods.

3.2.2 Suspended Sediment Concentrations

Time series of suspended sediment concentrations calculated for Sites B1B and 1M are shown in Figures 3.18a and 3.18b. Sediment concentration is estimated at 36 cm above the bed, corresponding to the elevation of the OBS sensors. Sediment concentrations are closely correlated with the shear

3.30
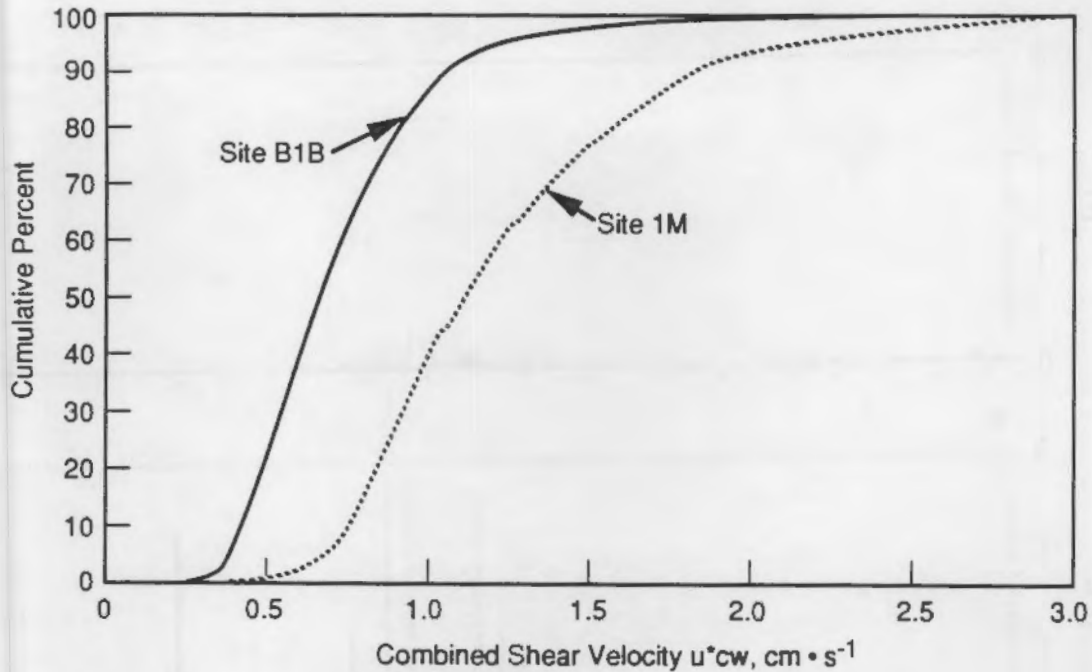
FIGURE 3.17. Cumulative Probability Distributions of Calculated Shear
Velocity $u*_{cw}$ at Sites B1B and 1M

velocity in excess of $1 \ cm \cdot s^{-1}$ because the calculations assumed critical
shear velocities near $1 \ cm \cdot s^{-1}$ for most of the sediment size classes at both
sites (Volume 2, Appendix C). Calculated sediment concentrations,
therefore, are also well correlated with the time series of wave-orbital
velocities used as input in the calculations, re-emphasizing the importance
of waves in causing sediment resuspension. The suspended sediment concentra-
tion time series is composed of numerous short-duration events. The events
have time scales equal to those of the shortest meteorological time scales;
virtually all resuspension events last less than 4 days, and many occur over
a few hours when waves and, for example, peak tidal currents combine to
produce sufficient shear velocities for resuspension. Estimated suspended
sediment concentrations are, overall, about 20 times higher at Site 1M than
at Site B1B. This is primarily a result of the higher shear velocities
calculated for Site 1M.

3.31
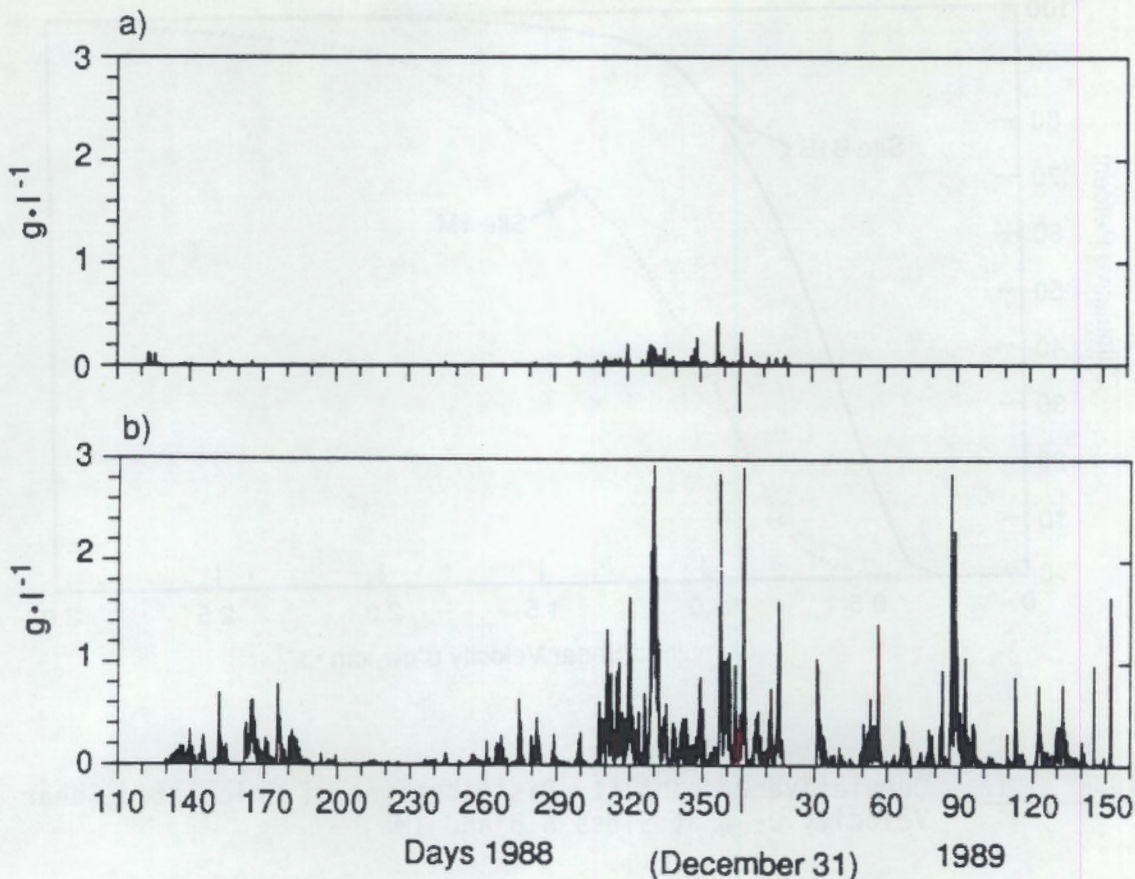
FIGURE 3.18. Calculated Suspended Sediment Concentration at 36 cm Above the Bottom at a) Site B1B and b) Site 1M

3.2.3 Suspended Sediment Flux

Hourly suspended sediment flux was calculated as the product of instantaneous sediment concentration and instantaneous current velocity, summed for elevations below 10 m. The hourly direction of sediment flux, therefore, corresponds exactly with the direction of the hourly current used as input to the calculations, but the rate of sediment flux depends on current speed and the sediment concentration. Thus, over periods of more than an hour, the mean flux direction can differ markedly from the mean current direction, because it depends on the timing of resuspension events relative to the currents.

3.32

a) Cumulative Alongshore Sediment Flux at Site B1B

b) Cumulative Cross-Shelf Sediment Flux at Site B1B

Days 1988   (December 31)   1989
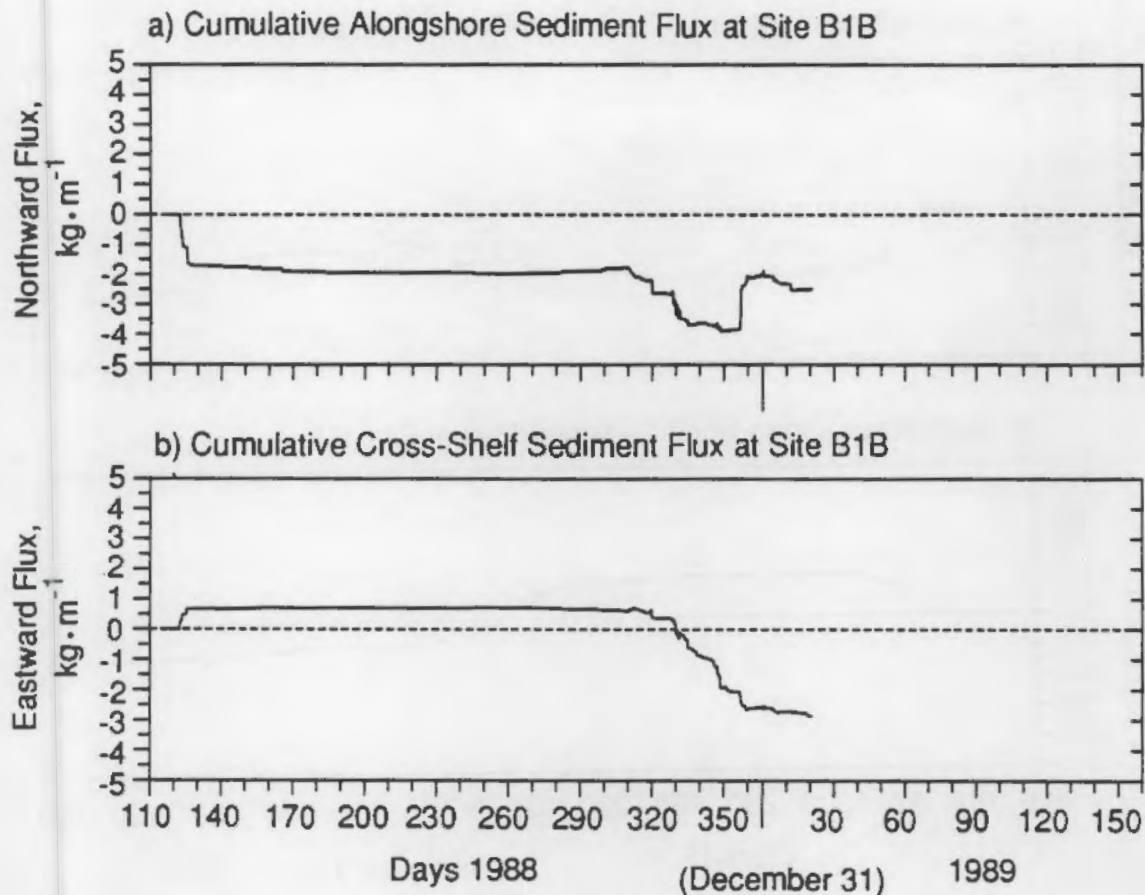
FIGURE 3.19.   Calculated Cumulative Alongshore and Cross-Shelf
Sediment Flux at Site B1B

The cumulative alongshore and cross-shelf components of sediment flux at
Sites B1B and 1M are plotted in Figures 3.19 and 3.20, and provide an indi-
cation of the net transport over the calculation period. Most resuspension
events are oscillatory; sediment is resuspended over several tidal cycles and
is advected by the tidal currents during the period of resuspension
(Volume 2, Appendix C). Calculated flux rates associated with individual
events were 10 to 20 times higher at Site 1M than rates during the same
events at Site B1B. The higher flux rates calculated at Site 1M are asso-
ciated with generally higher suspended sediment concentrations, not the
slightly greater current speeds.

3.33

a) Cumulative Alongshore Sediment Flux at Site 1M

b) Cumulative Cross-Shelf Sediment Flux at Site 1M

Days 1988   (December 31)   1989
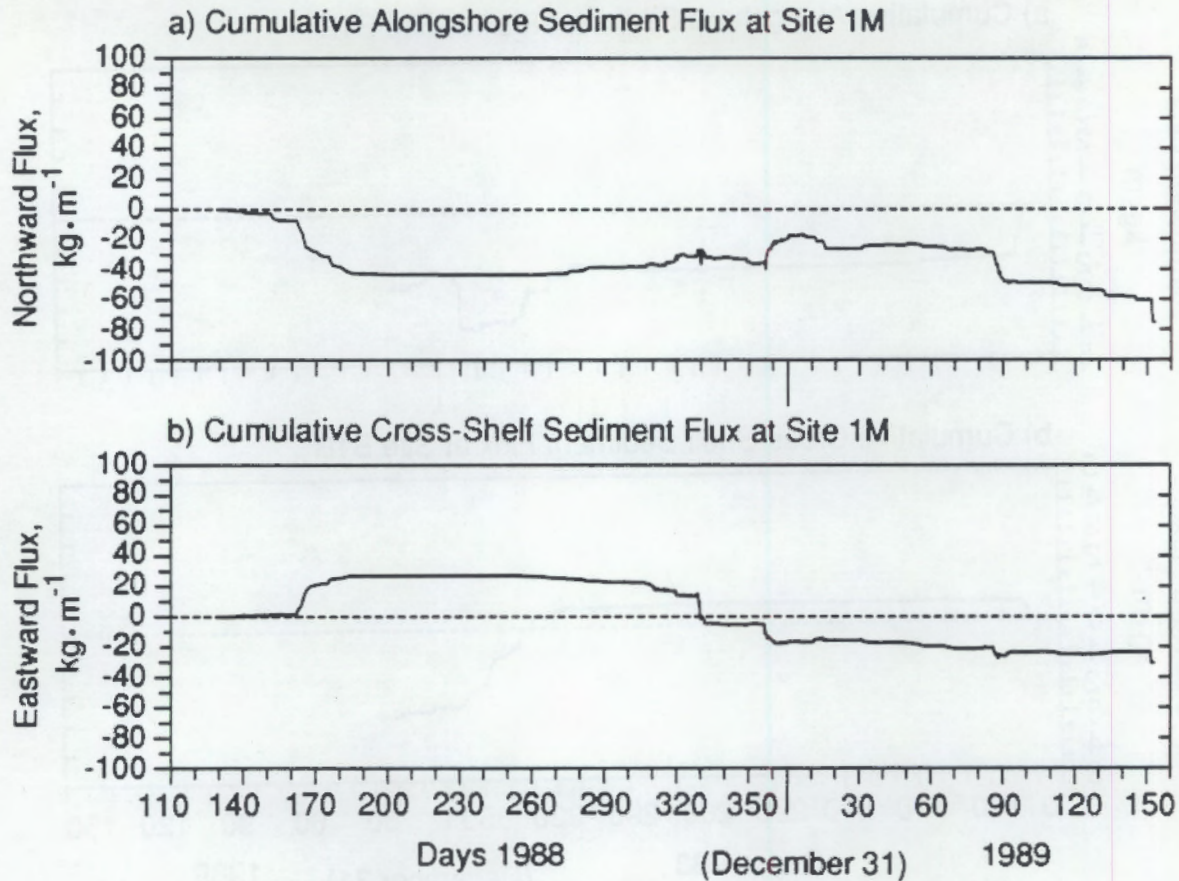
FIGURE 3.20. Calculated Cumulative Alongshore and Cross-Shelf Sediment Flux at Site 1M

Calculated net sediment transport for the deployment period at Site B1B was southward at 2.5 $kg \cdot m^{-1}$ and offshore at nearly 3.0 $kg \cdot m^{-1}$, but virtually all of the net alongshore transport can be accounted for by one event in April 1988 (near day 120). Although calculated flux rates were highest during the winter resuspension events, they resulted in very little net alongshore transport. Net alongshore transport to the north would have resulted if any of the larger southward-transport events had not occurred, but southward alongshore transport might have been higher if a longer current meter record allowed calculations during late winter and spring 1989. In other words, because the calculated net alongshore transport depends so heavily on individual events, it could easily change in a different year. In contrast, however, offshore transport occurred consistently during each resuspension event and probably represents a more certain long-term trend.

3.34

The cumulative transport curve calculated for Site 1M has a shape similar to that of Site B1B. A spring resuspension event associated with a strong southward current caused initial southward and onshore transport (Figure 3.20). Winter events through early January produced little net alongshore transport and caused additional offshore transport. A calculated resuspension event in late March 1989 (beginning around day 83) caused additional southward transport but only slight alongshore transport. Two final events associated with anomalous current speeds produced additional southward, offshore transport. Calculated net sediment transport at Site 1M was southward at 76 kg·m^{-1} and offshore at about 30 kg·m^{-1}. Strong currents measured at the beginning of the second deployment and near the end of the study period resulted in sediment transport, but their contribution to the cumulative transport is small.

3.2.4 Summary of Sediment Transport Calculations

Trends in long-term sediment fluxes calculated for Sites B1B and 1M are summarized in Figure 3.21, which shows the principal axes of variation (principal components) in calculated sediment fluxes after filtering with a 40-h low-pass filter (described in Volume 2, Appendix B). The vector of the long-term mean is also plotted as an arrow. Also plotted for each site in Figure 3.21 are the long-term mean current vectors and the principal axis of the M2 tidal ellipse. Note that, because of the malfunction of the current meter near the bottom at Site B1B during the last deployment, data and sediment transport calculations at Site B1B are based on a shorter period.

The principal axis of variation for sediment flux at Site B1B is rotated slightly clockwise (346°T) relative to the alongshore axis defined in this report (328°T), and the principal axes are closely aligned with the principal axes of the 40-h low-pass filtered currents from Site B1B. Likewise, the mean sediment flux is closely aligned with the mean current vector: mean sediment flux is southward and slightly offshore (197°T) at 0.016 g·cm^{-1}·s^{-1}. Mean currents for the study period were also southward and offshore (204°T) at 0.85 cm·s^{-1}. At Site B1B, calculated direction and variance in sediment transport direction correlates well with direction and variance in the long-term mean flow and low-frequency current variation.
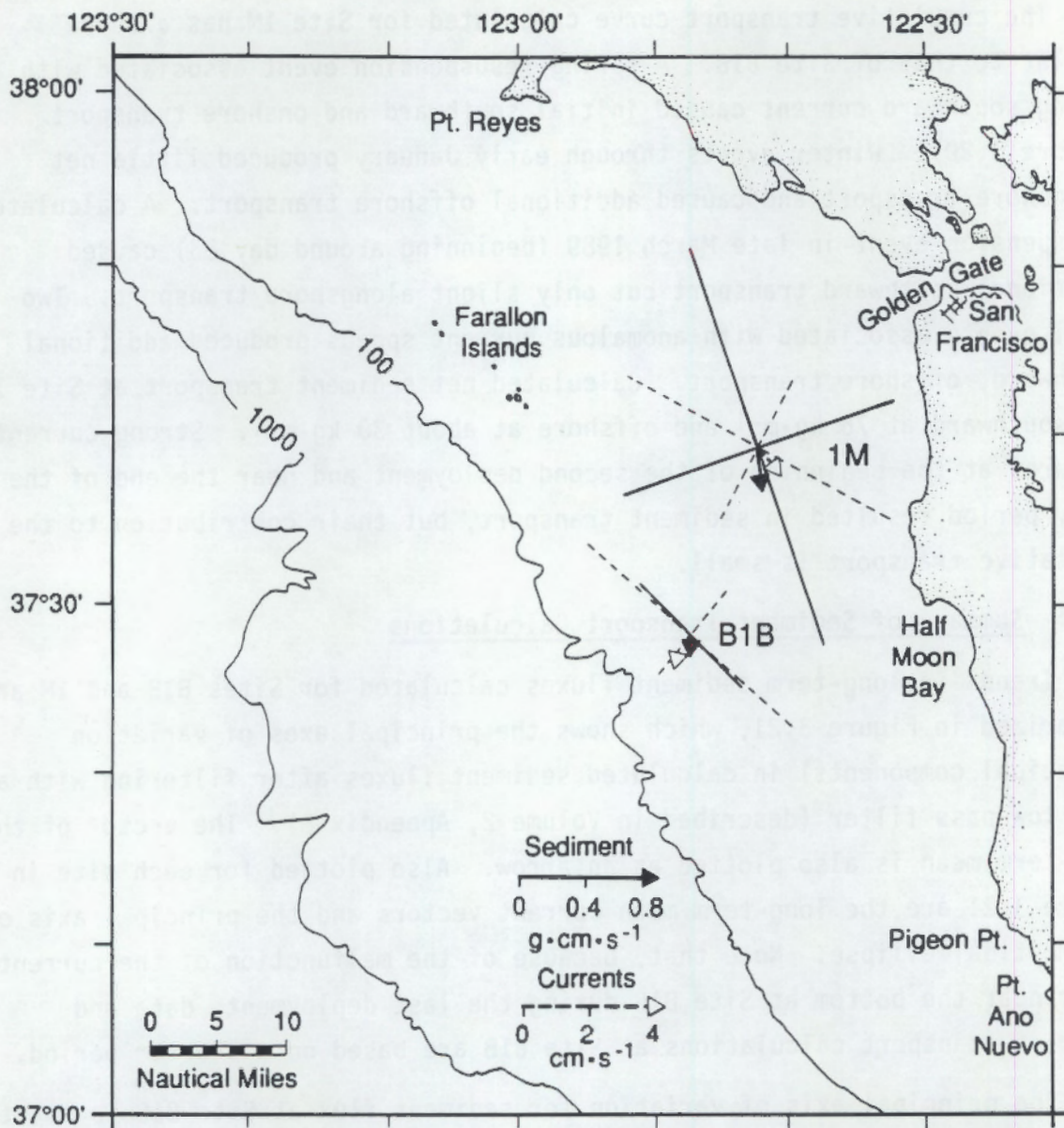
FIGURE 3.21. Summary of Mean and Principal Axes of Variation for Near-Bottom Current Velocity (dashed) and Calculated Sediment Fluxes (solid) at Sites B1B and 1M

At Site 1M, calculated mean sediment flux is southward (170°) with a very slight offshore component. The mean rate is 0.26 g·cm⁻¹·s⁻¹, about fifteen times higher than the mean rate at Site B1B. The direction of sediment flux contrasts with the mean current direction, which was southward with a substantial onshore component (1.12 cm·s⁻¹ toward 126°T). The

3.36

FIGURE 3.21. Summary of Mean and Principal Axes of Variation for Near-Bottom Current Velocity (dashed) and Calculated Sediment Fluxes (solid) at Sites B1B and 1M

At Site 1M, calculated mean sediment flux is southward (170°) with a very slight offshore component. The mean rate is 0.26 $g \cdot cm^{-1} \cdot s^{-1}$, about fifteen times higher than the mean rate at Site B1B. The direction of sediment flux contrasts with the mean current direction, which was southward with a substantial onshore component (1.12 $cm \cdot s^{-1}$ toward 126°T). The

3.36

principal axes of variation for the calculated sediment fluxes (341°T) are rotated clockwise about 43° relative to those for currents (298°T). The differences in low-pass filtered currents and sediment fluxes at Site 1M suggest that higher-frequency variations in current speed during times of sediment suspension are responsible for the mean sediment flux. In other words, tidal variations in currents make a larger contribution to the fate of material transported from Site 1M than they do at Site B1B. This is consistent with the larger diurnal tides observed at Site 1M (Volume 2, Appendix B).

3.3 OPTICAL BACKSCATTERANCE DATA

Suspended sediment concentrations were estimated using optical back-scatterance (OBS) sensors mounted 36 cm above the bottom. Previous experiments with these instruments deployed in San Francisco Bay (Sternberg et al. 1986), on the California continental shelf (Sherwood and Sternberg 1989), and in the nearshore zone (Downing 1983) have successfully measured wave-induced resuspension of silt and sand. Unfortunately, the OBS data acquired during this study were extremely noisy. The OBS sensor, electronics, and data logger appear to have worked well, and the large fluctuations and significant drift observed in the data are apparently related to physical phenomena near the bottom. Although several hypotheses for the OBS observations are presented in Volume 2, Appendix C, none are completely satisfactory. Because fairly arbitrary procedures were required to remove spikes and offsets in the data (Volume 2, Appendix B), confidence in resultant suspended sediment estimates is low. These data are further discussed in Volume 2, Appendix C.

coefficient of variation for the calculated sediment fluxes (31%) are
less than about 42% relative increase for currents.

Low-pass filtered currents and sediment fluxes at Site 1 show
that high-frequency variations in suspended-sediment flux, in either
tidal variations in currents, make a larger contribution to the flux of
suspended sediment at Site 1 (Bay Cove; Site 51b, Table) than
the larger diurnal tides observed at Site 1A (Figure 2.

BACKSCATTER DATA

Suspended-sediment concentrations have associated optical back-
scatterance (OBS) sensors mounted in situ of the bottom. This has experi-
ence with those instruments deployed in San Francisco Bay (Sternberg et al.,
1986). In some estuaries continue to shift (Smith and Stearns 1989) and
in the nearshore zone (Downing 1983) have successfully measured wave-induced
resuspension of silt and sand. Unfortunately, the OBS data acquired during
this study were extremely noisy. The OBS sensor electronics, and data
logger, appear to have worked well, and the large fluctuations (and variations)
observed in the data are apparently related to physical phenomena near
the sensor. Although several hypotheses for the OBS observations
presented in Volume 2, Appendix C, are incompletely satisfactory, because
calibration procedures were run prior to remove spikes and off-sets in the
data (Volume 2, Appendix B). Confidence in resultant suspended-sediment
estimates is low. These data are further discussed in Volume 2 Appendix C.

4.0 DISCUSSION

4.1 CURRENTS IN THE GULF OF THE FARALLONES

The year-long measurements performed in this study allow one of the first analyses of seasonal variation in currents on the continental shelf offshore San Francisco. This section reviews the seasonal circulation patterns proposed by Chelton (1984), based on his analysis of 20 years of CalCOFI hydrographic data, and compares them with data obtained during this study.

Chelton (1984) determined that a seasonal reversal in alongshore flow occurs at CalCOFI Station 67.57 (located offshore Monterey, California). The surface flow is strongly southward from March through June and more weakly southward from September through November. Weak northward flow occurs during the rest of the year. Hydrographic data obtained north of Monterey indicate similar seasonal flow patterns. This circulation pattern is consistent with the hypothesis that the southward jet associated with upwelling reverses the northward flow of the Davidson Current during spring/summer, creating south-ward flow at the surface and a northward flow at depth (the Poleward Under-current; see Section 1.3.1). During fall/winter the Davidson Current flow is northward at all depths. The monthly mean flow velocities from CCCCS Mooring K and SuperCODE Mooring H3 support this hypothesis (Figure 4.1).

The measurements made at Sites B1B and 1M are not consistent with the circulation pattern proposed by Chelton (1984). At Site B1B, there is no evidence for the northward Davidson Current flow at the surface in fall/winter (Figure 3.7). Although strong southward flow was measured in spring at Site B1B, strong southward flow also occurred during some fall/winter months. Weak northward flow occurred near the bottom during 4 months, evenly distributed among the two seasons. Overall, there is substantially less northward flow at Site B1B than is expected from Chelton's circulation pattern.

At Site 1M, the situation is more complicated. During spring/summer, the surface flow was northward (instead of southward, as predicted) and the deeper flow was southward (instead of northward). The situation reversed in
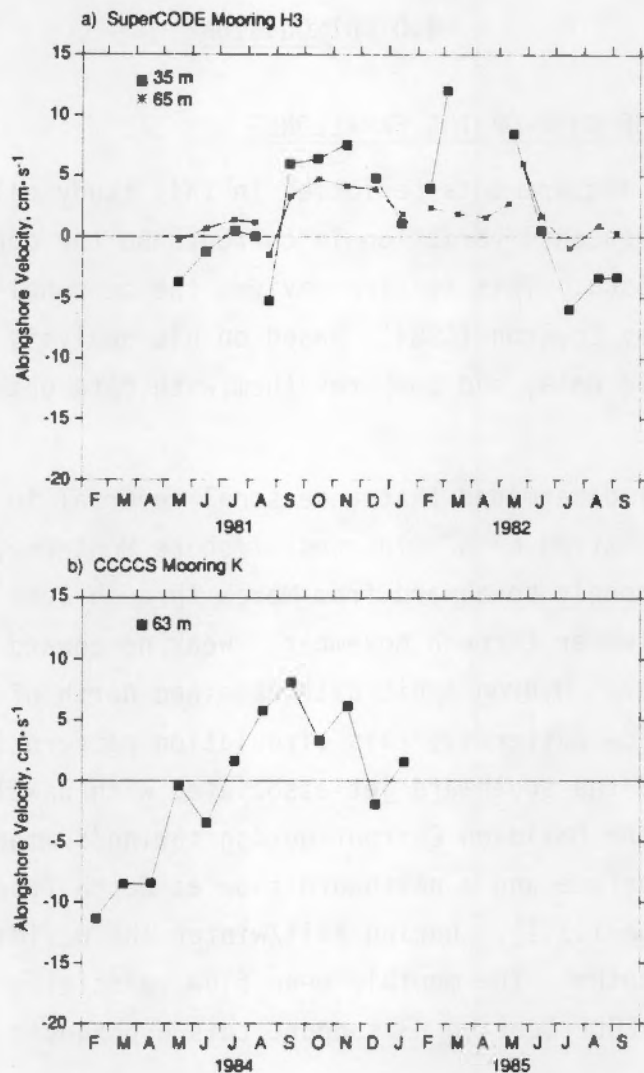
FIGURE 4.1. Monthly Mean Alongshore Current Velocities at a) SuperCODE
Mooring H3 (Denbo and Allen 1987) and b) CCCCS Mooring K
(Chelton et al. 1988)

the fall/winter, when southward mean flow occurred at the surface (instead of
the northward Davidson Current) and northward flow occurred at the bottom.
Some aspects of the circulation at Site 1M are certainly related to its loca-
tion in shallow water, closer to the entrance to San Francisco Bay. The
long-term mean near-surface and near-bottom currents are in opposite direc-
tions, despite the high coherence estimated in the wind-forced and tidal
frequency bands (Figure 3.14). This reversal of near-surface and near-bottom

flow direction may be indirect evidence for the influence of salinity-induced stratification caused by freshwater discharge from San Francisco Bay. More direct evidence of the influence of tidal exchange through the Golden Gate was provided by the orientation of the M2 tidal ellipses at Site 1M. An overall increase in tidal influence at Site 1M, compared with Site B1B, is consistent with a general increase in tidal amplitude with shallower water depths and proximity to the Golden Gate. The data from the SWOOP current meter mooring, which is located inshore of Site 1M, show even greater tidal influence (Roberts 1980) and are consistent with this pattern.

The response of currents at both sites to local winds was more typical of other observations made along the California coast. Although cross-spectral analysis indicates that statistically significant correlation exists among measured currents and local winds represented by the NDBC Buoy 46012 data, only about half of the observed current fluctuations occurring over periods of 2 to 10 days can be related to local winds. The best correlation was found among the alongshore components of currents and wind stress. These results are consistent with relationships observed at Moorings K and H3, and at the CODE site (Denbo and Allen 1987; Chelton et al. 1988; Davis and Bogden 1989).

4.2 SEDIMENT TRANSPORT AT SITES B1B AND 1M

This study presents sediment transport calculations made using a sophisticated wave-current boundary layer model and frequently sampled, site-specific data for waves and currents. Estimation of sediment transport is, however, notoriously difficult, and there is substantial uncertainty surrounding the transport estimates. The likely sources of error and the sensitivity of the results to uncertainty are discussed in detail in Volume 2, Appendix C. The greatest uncertainty is associated with the frequency of resuspension and the rate of transport, because in the calculations these are affected by characteristics of the bottom material that are difficult to determine (critical shear stress and settling velocity) and a reference concentration coefficient (γ_0) for which a large range of values has been proposed. More certain are the calculated transport directions,

4.3

which depend strongly on the measured currents. The greatest confidence is placed in comparisons made between the two sites.

The following section discusses the physical differences between the two sites and their effects on transport of material from each site. Section 4.2.2 compares the results of this study to those of an earlier study that used a different approach for calculating dispersion of sediment from the sites.

4.2.1 Comparison of the Two Candidate Sites

Depth

Depth is the most important difference between the two sites. The shallower depth at Site 1M allows more wave energy to reach the bottom and results in more frequent, longer-duration resuspension events. As the dredged material accumulates in mounds at the sites, the depth difference will become even more pronounced because the amount of wave energy that reaches the bottom will be relatively greater at Site 1M. For example, Table 1.1 indicates that the near-bottom wave-orbital velocity under a 3-m, 14-s wave in water 80 m deep is 24 $cm \cdot s^{-1}$, and in water 50 m deep is 43 $cm \cdot s^{-1}$. Decreasing the water depth by 10 m at both sites increases orbital velocity by 5 $cm \cdot s^{-1}$ (to 29 $cm \cdot s^{-1}$) at the deeper site, but at the shallower site, the 10-m-depth change produces a 11-$cm \cdot s^{-1}$ increase to 54 $cm \cdot s^{-1}$. This implies that, if dredged material accumulated at Sites B1B and 1M at equal rates, transport rates at Site 1M would increase more rapidly than at Site B1B. If the material placed at the sites was similar, it would be resuspended more frequently at Site 1M.

Wave Climate

Wave energy is primarily responsible for resuspending bottom material and making it available for transport by currents. In this study, identical wave climates were assumed for Sites B1B and 1M. The degree to which Montara wave data represent conditions at the two sites is difficult to ascertain. The Montara wave data for the study period indicate smaller wave heights and shorter periods than wave climate estimates prepared by Tetra Tech (1987), based on hindcasts from 20 years of data (Corson et al. 1986). Assuming

that the Tetra Tech calculations represent the long-term wave climate at the two locations, the discrepancy may mean that the study was conducted during a period of milder wave conditions, or it may mean that the Montara data are unsuitable for making reliable estimates at the two sites without correcting for shoaling effects. The Tetra Tech calculations indicate that the wave climate is more severe (higher waves, longer periods) at Site B1B than at Site 1M. This difference would tend to increase the calculated frequency and rate of transport at Site B1B. Even fairly large increases in the wave climate at Site B1B are unlikely to change the relative transport rates between the two sites, because the difference is mostly due to the 44-m difference in water depth.

Continental Shelf Circulation

The data collected in this study indicates that the two candidate sites are located in different current regimes. Although the distributions of measured near-bottom current speed were very similar at the two sites, tidal analysis indicated that tidal currents are stronger at Site 1M and show influence of tidal exchange through the Golden Gate. Tidal currents at Site B1B are slightly weaker and more rotary. Among the current meter data from the five instrument locations, data from the near-bottom currents at Site B1B were most coherent with the wind data and best aligned with the bottom contours. Overall, the near-bottom currents at Site B1B appear to respond more to wind forcing than at Site 1M. The implications for sediment transport are 1) transport at Site B1B is mostly parallel with the depth contours and strongly influenced by seasonal and long-term mean current directions, but 2) at Site 1M, transport directions do not correspond well with local depth contours and are more influenced by tides.

4.2.2 Comparison with the Results of Earlier Studies

The study performed by Tetra Tech (1987) estimated sediment dispersion from candidate Site B1 (located near B1B) and Site 1M. That study differs from the calculations presented in this report in two important respects: 1) wave and current statistics (in the form of probability distributions) were used as input for sediment transport calculations in the Tetra Tech study, rather than time series of measurements, and 2) only bedload sediment

4.5

transport calculations were made in the Tetra Tech study, neglecting sus-
pended sediment transport except during disposal operations. The present
calculations benefit from the measurements made at the candidate sites during
this study, and allow calculations of hourly sediment transport that combine
wave- and current-induced resuspension events with hourly current speed and
direction. The direction of sediment transport calculated in this study can,
therefore, differ from the mean current direction, because transport direc-
tion depends also on the timing of resuspension. In many other respects, the
calculations and predictions are similar. As pointed out in the Tetra Tech
report, the large uncertainty surrounding critical shear stress values
appropriate for dredged material remains a problem. However, the common
conclusions of both studies do not depend on the value of critical shear
stress. They are

- Some transport will occur at both candidate sites, but transport
  rates are much higher (10 to 20 times greater) at Site 1M.

- Transport rates are dominated by the wave climate and water depth,
  and transport rates will increase in shallower water depths.

In addition, this study and the Tetra Tech study both predict onshore
transport at Site 1M, but for different reasons. In the Tetra Tech study,
transport direction was influenced by the Stokes drift in the direction of
wave transport. In this study, transport direction is determined by current
direction and timing of resuspension.

The present study validates some of the assumptions used in the Tetra
Tech study. In particular, the M2 tidal ellipse calculated in this study is
elongate toward the Golden Gate and confirms that Site 1M is influenced by
tidal exchange with San Francisco Bay. An assumption made in the Tetra Tech
study that was not confirmed by this measurement program is that mean current
direction at Site B1B can be well represented by the Mooring K measurements.
As discussed above, substantial differences were observed.

A significant difference in the conclusions of the two studies exists in
the calculated transport directions at Site 1M. The Tetra Tech study pre-
dicted northward, onshore movement of material deposited at Site 1M; this

4.6

study predicts southward, onshore movement. The difference arises from the methods used for calculating sediment transport direction.

4.3 INTERANNUAL VARIABILITY

The issue of interannual variability (year-to-year changes) is important when extrapolating the results of this study to make longer-term predictions regarding the fate of dredged material. The question can be simply stated: Are the conditions measured during this 13-month study representative of the means and extremes likely to occur over the lifetime of the disposal sites? Interannual variability occurs in winds, currents, and waves, and will result in differences in sediment transport from year to year. In particular, the frequency and severity of the storms that ultimately dominate sediment transport will vary. The results and calculations of this report are valid only to the degree that the study period represents the long-term conditions.

The factors with the greatest effect on sediment transport calculations are the frequency of high, long-period waves, and the direction of the currents. Wave climate was discussed in Section 1.4.4. Long-term wave data are not available for Montara, and only a few years of data are available from CDIP for the Farallon Island waverider buoy. Although long-term data are available for other nearby sites, published data for the study period are not yet available. It is difficult, therefore, to determine how well the wave data used in these calculations represent the long-term conditions.

The direction of sediment transport calculated in Section 3.3 is very sensitive to the mean current direction, particularly during the winter-storm season. The seasonal current variations measured in this study are different from those measured slightly to the south, at Moorings K and H3, where mean northward flow was measured. Because data from those moorings were obtained at different locations, and in different years, two hypotheses for the difference in currents are equally possible: 1) the current patterns are different for reasons of location or 2) the current patterns are different because of interannual variation. Because the H3 mooring was located at the same depth and less than 20 km from Site B1B, there is no reason to expect

4.7

that currents at H3 should differ greatly from those at Site B1B. Thus, it seems more probable that the discrepancy between mean flows at Sites B1B and H3 is due to interannual variability. The implication for sediment transport calculations is that less southward sediment transport, or possibly northward transport, could occur in other years. At Site 1M, the only data available are from this study and, although it is clear that spatial differences exist between Site 1M and Site B1B, the potential for year-to-year variation in the currents cannot be assessed. The important issue of interannual variability in currents at the candidate sites can only be addressed with longer-term measurements.

5.0 CONCLUSIONS

This report has described a physical oceanographic measurement program conducted at two candidate dredged-material disposal sites in the Gulf of the Farallones offshore San Francisco. Data were collected for a nearly continuous 13-month period between April 1988 and May 1989. Subsequent analysis of the data and estimation of sediment transport at the two sites were performed, and the results are contained in this report. The important conclusions from this study are listed below.

5.1 CURRENTS

Current velocities were measured at depths of 21 m, 46 m, and 85 m at Site B1B (86-m water depth), and at depths of 21 m and 40 m at Site 1M (42-m water depth). The following conclusions were drawn from analysis of the current meter data.

- The mean alongshore component of currents was southward at both sites and all depths except at 21 m at Site 1M, where the alongshore mean was northward. The mean cross-shelf component was onshore at both sites and all depths except at 85 m at Site B1B, where it was offshore. Mean currents for the entire data set are summarized in Figure 3.10 and Table 3.1.

- Seasonal variations in the strength of the alongshore currents occurred at Site B1B, but flow was southward at all depths and in both spring/summer and fall/winter seasons. Seasonal reversals of flow occurred at Site 1M. In spring/summer, alongshore flow was southward near the bottom (40 m) and northward at 21 m. In fall/winter, the opposite occurred, and mean flow was northward near the bottom and southward at 21 m. Seasonal flows are summarized in Table 3.2.

- Low-frequency currents were mostly aligned with the regional bathymetric contours at both sites, as indicated by the principal components. Cross-shelf variation decreased with depth at both sites, and the orientation of the principal (alongshore) axis rotated counterclockwise with depth.

- Tidal currents were predominantly cross-shelf at both sites. Tidal currents were stronger at Site 1M, and the diurnal M2 tidal ellipse was oriented toward the entrance to San Francisco Bay. Tides at Site B1B were weaker and more rotary in nature. Tidal currents accounted for approximately 50% of the variance in current velocity at Site B1B and about 70% of the variance at Site 1M.

- Cross-spectral analyses of the current meter data indicated low, but statistically significant, coherence in the wind-forced frequency band for the alongshore components of velocity. The cross-shelf components of currents at the two sites were not coherent. Changes in the alongshore component of low-frequency flow occurred first at Site 1M.

- Cross-spectral analyses between the wind at NDBC buoy 46012 and the currents indicated moderate, statistically significant coherence at periods of 2 to 10 days. Wind-driven flows accounted for 40% to 50% of the variance in current velocities at these long periods.

- Currents at both sites differed from the accepted continental shelf circulation pattern described by previous researchers. At Site B1B, the seasonal pattern was different from that observed at nearby moorings, and surprisingly little northward flow was observed. A likely explanation is that significant interannual variation occurs at Site B1B. At Site 1M, reversal in the mean current with depth occurred, suggesting that processes associated with stratification were important. The increased tidal influence and the greater variability observed at Site 1M suggest that currents at that site were more strongly influenced by the coastal boundary and flow around headlands, points, and bays, as well as tidal flow through the Golden Gate.

5.2 SEDIMENT TRANSPORT

Sediment-transport calculations were performed using a wave-current boundary layer model, measured current velocities, and wave parameters estimated from data recorded at Montara. The calculations predicted the vertical profiles for sediment concentration and velocity, and estimated rates and directions of suspended-sediment transport. The following conclusions were drawn from the calculations.

- Resuspension of bottom material was caused primarily by wave action. Measured currents alone were seldom sufficient to cause resuspension and transport, but isolated incidents of strong currents, which caused sediment transport, were recorded. Strong, near-bottom currents occurred more often in the winter storm season, probably because 1) stronger winds were present and 2) the water column was well mixed and wind-driven surface currents were more closely coupled with near-bottom currents.

- Resuspension of sediment occurred much more frequently in fall/ winter, when long-period swell from distant storms and shorter-period wind waves from intense local storms both caused higher wave-orbital velocities near the bottom.

- Resuspension occurred more frequently at the shallower Site 1M because 1) energy from shorter-period waves can reach the bottom and 2) more energy from waves of all periods can reach the bottom.

- Because resuspension occurred more frequently, and because more sediment is suspended, calculated transport rates at Site 1M are approximately 10 to 20 times higher than transport rates at Site B1B. In addition, because more energy reached the bottom at Site 1M, material can be transported that would remain immobile at Site B1B.

- Calculated net transport at both sites is southward and offshore. At Site B1B, the mean transport direction corresponds closely with the mean current direction. At Site 1M, calculated mean sediment transport diverges from the mean current direction, which has a substantial onshore component. Because the transport calculations at Site 1M are based on a longer record and depend less on individual events, reasonable confidence is associated with the calculated southward direction for net transport. In contrast, less confidence is placed on the calculations made at Site B1B because 1) the period of data for calculations is 120 days shorter and 2) the sign of the calculated alongshore component of sediment transport can be changed by omitting key individual transport events.

- Finally, there are uncertainties inherent in these sediment transport calculations. These uncertainties arise from several sources, the most important of which are simplifying assumptions made in determining suspended sediment concentration, uncertainty in the value of critical shear stress, and large spread in values for other empirically established coefficients. Greatest uncertainty in the calculated results is associated with the magnitude of the flux, which may be in error by a factor of 10. The direction of transport is more certain especially at Site 1M. The greatest confidence is placed in comparisons between the two sites. Unless the Montara wave data provide a very poor representation of conditions at one of the two sites, it is apparent from these calculations that material will disperse more rapidly from Site 1M than from Site B1B.

6.0 REFERENCES

Allen, J. S., R. C. Beardsley, J. O. Blanton, W. C. Boicourt, B. Butman, L. K. Coachman, A. Huyer, T. H. Kinder, T. C. Royer, J. D. Schumacher, R. L. Smith, W. Sturges, and C. D. Winant. 1983. "Physical Oceanography of Continental Shelves." Reviews of Geophysics and Space Physics 21:1149.

CDIP. 1988. Monthly Summary Reports, Coastal Data Information Program, Ocean Engineering Research Group, Institute of Marine Resources, Scripps Institute of Oceanography, La Jolla, California.

CH2M Hill, E2 Consulting Engineers, Romov-Underwater Resources, Monterey Vessels, and P. J. W. Roberts. 1989. Wastefield Transport and Bacteriological Compliance Studies of the San Francisco Ocean Outfall. Report to U.S. Environmental Protection Agency and San Francisco Bay Regional Water Quality Control Board, San Francisco, California.

Chelton, D. B. 1984. "Seasonal Variability of Alongshore Geostrophic Velocity Off Central California." Journal of Geophysical Research 89:3473-3486.

Chelton, D. B., A. W. Bratkovich., R. L. Bernstein, and P. M. Kosro. 1988. "Poleward Flow Off Central California During the Spring and Summer of 1981 and 1984." Journal of Geophysical Research 93(C9):10,604-10,620.

Corson, W. D., C. E. Abel, R. M. Brooks, P. D. Farrar, B. J. Groves, R. E. Jensen, J. B. Payne, D. S. Ragsdale, and B. A. Tracy. 1986. Pacific Coast Hindcast Deepwater Wave Information. Final Report. Wave Information Studies of U.S. Coastlines, WIS Report 14. U.S. Army Corps of Engineers, Coastal Engineering Research Center, Waterways Experiment Station, Vicksburg, Mississippi.

Davis, R. E. 1985. "Drifter Observations of Coastal Surface Currents During CODE: The Method and Descriptive View." Journal of Geophysical Research 90:4741-4755.

Davis, R. E. and P. S. Bogden. 1989. "Variability on the California Shelf Forced by Local and Remote Winds During the Coastal Ocean Dynamics Experiment." Journal of Geophysical Research 94(C4):4763.

Denbo, D. W. and J. S. Allen. 1987. "Large-scale Response to Atmospheric Forcing of Shelf Currents and Coastal Sea Level Off the West Coast of North America." Journal of Geophysical Research 92:1757-1782.

Denbo, D. W., K. Polzin, J. S. Allen, A. Huyer, and R. L. Smith. 1984. Current Meter Observations Over the Continental Shelf Off Oregon and Northern California, February 1981-January 1984. Data Report 112, College of Oceanography, Oregon State University.

Downing, J. P. 1983. "An Optical Instrument for Monitoring Suspended Particles in Ocean and Laboratory." Institute of Electronic and Electrical Engineers and Marine Technology Society. In Proceedings of OCEANS '83, pp. 199-202, San Francisco.

Downing, J. P., and R. A. Beach. 1989. "Laboratory Apparatus for Calibrating Optical Suspended Sediment Solids Sensors." Marine Geology 86:243-249.

Earle, M. D., K. A. Bush, and G. D. Hamilton. 1984. "High-Height Long-Period Ocean Waves Generated by a Severe Storm in the Northeast Pacific Ocean During February 1983." Journal of Physical Oceanography 14:1286-1299.

Foreman, M. G. G. 1978. Manual for Tidal Currents Analysis and Prediction. Pacific Marine Science Report 78-6 (May 1984 Edition), Institute of Ocean Sciences, Sidney, B.C., Canada.

Grant, W. D., and O. S. Madsen. 1979. "Combined Wave and Current Interaction With a Rough Bottom." Journal of Geophysical Research 84(C4): 1797-1808.

Grant, W. D., and O. S. Madsen. 1986. "The Continental Shelf Bottom Boundary Layer." Annual Review of Fluid Mechanics 18:265-305.

Halliwell, G. R. Jr., and J. S. Allen. 1987. "The Large-Scale Sea Level Response to Atmospheric Forcing Along the West Coast of North America, 1981-1982." Journal of Geophysical Research 92:1861-1884.

Hickey, B. M. 1979. "The California Current System: Hypothesis and Facts." Progress in Oceanography 8:191-279.

Huyer, A. 1983. "Coastal Upwelling in the California Current System." Progress in Oceanography 12:259-284.

Huyer, A. 1990. "Shelf Circulation." In The Sea: Ocean Engineering Science, Vol. 9. pp. 423-466, B. Le MeHaute and D. M. Hanes, eds, Wiley and Sons, Inc., New York, New York.

Huyer, A., and R. L. Smith. 1985. "The Signature of El Nino Off Oregon, 1982-1983." Journal of Geophysical Research 90:7133-7142.

Jenkins, G. M., and D. G. Watts. 1968. Spectral Analysis and Its Applications. Holden-Day, San Francisco.

Kachel, N. B., and J. D. Smith. 1986. "Geological Impact of Sediment Transporting Events on the Washington Continental Shelf." In Shelf Sands and Sandstones, pp. 145-162, Canadian Society of Petroleum Geologists Memoir 2, Calgary, Ontario, Canada.

Komar, P. D. 1976. Beach Processes and Sedimentation. Prentice-Hall, Inc., Englewood Cliffs, New Jersey.

Larsen, L. H., R. W. Sternberg, N. C. Shi, M. A. H. Marsden, and L. Thomas. 1981. "Field Investigations of the Threshold of Grain Motion by Ocean Waves and Currents." Marine Geology 42:105-132.

Lynn, R. J., and J. J. Simpson. 1987. "The California Current System: The Seasonal Variability of Its Physical Characteristics." Journal of Geophysical Research 92:12,947-12,966.

NOS (National Ocean Survey). 1987. Tide Tables 1988; High and Low Water Predictions; West Coast of North and South America Including the Hawaiian Islands. National Oceanic and Atmospheric Administration, U.S. Department of Commerce, Rockville, Maryland.

NOS (National Ocean Survey). 1988. Tide Tables 1989; West Coast of North and South America. U.S. Department of Commerce, National Oceanic and Atmospheric Administration, Rockville, Maryland.

Nybakken, J., W. Borenkow, M. Silberstein, P. Slattery, A. R. Flegal, G. Knauer, R. Risebrough, and B. Antrim. 1983. Baseline Survey and Site Selection for Ocean Disposal, Gulf of the Farallones. Prepared for the Department of the Army, San Francisco District, Corps of Engineers, San Francisco, California, by Moss Landing Marine Laboratories, Moss Landing, California.

Reid, J. L., and R. A. Schwartzlose. 1962. "Direct Measurement of the Davidson Current Off Central California." Journal of Geophysical Research 67:2591.

Roberts, P. J. W. 1980. "Ocean Outfall Dilution: Effects of Currents." Journal of the Hydraulics Division 106, MY5:769-782.

Schwartzlose, R. A. 1963. Nearshore Currents of the Western United States and Baja, California, As Measured by Drift Bottles. CalCOFI Progress Report, 7/1/60 to 6/3/62.

Seymour, R. J., M. H. Sessions, and D. Castel. 1985. "Automated Remote Recording and Analysis of Coastal Data." Journal of Waterway, Port, Coastal, and Ocean Engineering 111(2):388-400.

Sherwood, C. R., and R. W. Sternberg. 1989. "Near-Bottom Suspended Sediment Measurements on the Northern California Continental Shelf - STRESS-1." EOS 70(43):1144.

Shi, N. C., L. H. Larsen, and J. P. Downing. 1985. "Predicting Suspended Sediment Concentrations of Continental Shelves." Marine Geology 62:155-175.

Sternberg, R. W., R. V. Johnson II, D. A. Cacchione, and D. E. Drake. 1986. "An Instrument System for Monitoring and Sampling Suspended Sediment in the Benthic Boundary Layer." Marine Geology 71:187-199.

Strub, P. T., J. S. Allen, A. Huyer, and R. L. Smith. 1987. "Large-Scale Structure of the Spring Transition in the Coastal Ocean Off Western North America." Journal of Geophysical Research 92:1527-1544.

Strub, P. T., J. S. Allen, A. Huyer, R. L. Smith, and R. C. Beardsley. 1987. "Seasonal Cycles of Currents, Temperatures, Winds and Sea Level Over the Northeast Pacific Continental Shelf: 35N to 48N." Journal of Geophysical Research 92:1507-1526.

Tetra Tech, Inc. 1987. Sedimentation and Dispersion Analysis, San Francisco Dredged Material Ocean Disposal Site Evaluation. Final Report prepared for U.S. Army Corps of Engineers, San Francisco, by Tetra Tech, Inc., San Francisco, California.

Winant, C. D., R. C. Beardsley, and R. E. Davis. 1987. "Moored Wind, Temperature, and Current Observations Made During Coastal Ocean Dynamics Experiments 1 and 2 Over the Northern California Continental Shelf and Upper Slope." Journal of Geophysical Research 92:1569-1604.

DISTRIBUTION

No. cf
Copies

No. of
Copies

OFFSITE

2   DOE/Office of Scientific and
Technical Information

R. Chisolm
U.S. Army Corps of Engineers
San Francisco District
211 Main St.
San Francisco, CA 94105

2   D. Coats
Marine Research Specialists
3639 E. Harber Blvd.
Ventura, CA 93001

P. Dragos
Battelle Ocean Sciences
397 Washington St.
Duxbury, MA 02332-0601

G. Gelfenbaum
U.S. Geological Survey
600 4th St. South
St. Petersburg, FL 33701

J. Harari
U.S. Army Corps of Engineers
San Francisco District
211 Main St.
San Francisco, CA 94105

C. Hunt
Battelle Ocean Sciences
397 Washington St.
Duxbury, MA 02332-0601

S. McDowell
Battelle Ocean Sciences
397 Washington St.
Duxbury, MA 02332-0601

M. Noble
U.S. Geological Survey
345 Middlefield Rd.
Menlo Park, CA 94025

5   D. Roberts
U.S. Army Corps of Engineers
San Francisco District
211 Main St.
San Francisco, CA 94105

R. Sternberg
Oceanography WB-10
University of Washington
Seattle, WA 98195

B. Walls
Battelle Ocean Sciences
397 Washington St.
Duxbury, MA 02332-0601

ONSITE

DOE Richland Operations Office

P. W. Kruger

31   Pacific Northwest Laboratory

D. W. Denbo (2)
J. P. Downing (2)
R. M. Ecker
J. W. Falco
W. R. Gorst
J. M. Hales
P. C. Hays
W. H. Pearson
W. T. Pennell
C. R. Sherwood (10)
R. L. Skaggs
J. A. Trelstad (2)
J. Q. Word
Publishing Coordination
Technical Report Files (5)